

# Phase-synchronized stimulus presentation augments contingency knowledge and affective evaluation in a fear conditioning task

<https://doi.org/10.1523/ENEURO.0538-20.2021>

**Cite as:** eNeuro 2021; 10.1523/ENEURO.0538-20.2021

Received: 4 December 2020

Revised: 15 October 2021

Accepted: 26 October 2021

---

*This Early Release article has been peer-reviewed and accepted, but has not been through the composition and copyediting processes. The final version may differ slightly in style or formatting and will contain links to any extended data.*

**Alerts:** Sign up at [www.eneuro.org/alerts](http://www.eneuro.org/alerts) to receive customized email alerts when the fully formatted version of this article is published.

Copyright © 2021 Plog et al.

This is an open-access article distributed under the terms of the Creative Commons Attribution 4.0 International license, which permits unrestricted use, distribution and reproduction in any medium provided that the original work is properly attributed.

**Title:** Phase-synchronized stimulus presentation augments contingency knowledge and affective evaluation in a fear conditioning task

**Abbreviated Title:** Phase-synchronization in fear conditioning

**Author names and affiliations:** Elena Plog<sup>1\*</sup>, Martin I. Antov<sup>1\*</sup>, Philipp Bierwirth<sup>1</sup>, Andreas Keil<sup>2</sup>, and Ursula Stockhorst<sup>1</sup>

<sup>1</sup>Institute of Psychology, Experimental Psychology II and Biological Psychology, University of Osnabrück, D-49074 Osnabrück, Germany (E. Plog, M. I. Antov, P. Bierwirth, and U. Stockhorst)

<sup>2</sup>Department of Psychology and Center for the Study of Emotion and Attention, University of Florida, Gainesville, Florida, 32611, USA

**Authors Contributions:** E. Plog designed research, performed research, analyzed data, wrote the paper (first draft); M.I. Antov designed research, performed research, analyzed data and wrote the paper (first draft); P. Bierwirth analyzed data, A. Keil, contributed analytic tools, wrote the paper, U. Stockhorst designed research and wrote the paper

\* These two authors contributed equally.

**Correspondence should be addressed to:** Elena Plog, D-49074 Osnabrück, E-Mail: [eplog@uni-osnabrueck.de](mailto:eplog@uni-osnabrueck.de)

Number of Figures: 8

Number of Tables: 1

Number of Multimedia: 0

Number of extended data: 11 figures

Number of words for Abstract: 249 words

Number of words for Significance Statement: 89

Number of words for Introduction: 748

Number of words for Discussion: 2749

**Acknowledgements:** We thank Jelena Gildehaus and Tabea Rasche for help with the recruitment of participants and data collection

**Conflict of Interest:** The authors declare no competing financial interests.

**Funding sources:** The study was supported by the research profile line "Cognition" of the University of Osnabrück, Germany

32 **Phase-synchronized stimulus presentation augments contingency knowledge and**  
33 **affective evaluation in a fear conditioning task**

34 **Abstract**

35 Memory often combines information from different sensory modalities. Animal studies show  
36 that synchronized neuronal activity in the theta band (4-8 Hz) binds multimodal associations.  
37 Studies with human participants have likewise established that theta-phase synchronization  
38 augments the formation of declarative video-tone pair memories. Another form of associative  
39 learning, classical fear conditioning, models non-declarative, emotional memory – with  
40 distinct neuronal mechanisms. Typical fear conditioning tasks pair a conditioned stimulus  
41 (CS) in one modality with an aversive unconditioned stimulus (US) in another. The present  
42 study examines the effects of CS-US synchronization in the theta band on fear memory  
43 formation in humans.

44 In a fear generalization procedure, we paired one of five visual gratings of varying orientation  
45 (CS) with an aversive auditory US. We modulated the luminance of the CS and the volume of  
46 the US at a rate of 4 Hz. To manipulate the synchrony between visual and auditory input  
47 during fear acquisition, one group (N = 20) received synchronous CS-US pairing, whereas  
48 the control group (N = 20) received the CS-US pairs out-of-phase.

49 Phase synchronization improved CS-US contingency knowledge and facilitated CS  
50 discrimination in terms of rated valence and arousal, resulting in narrower generalization  
51 across the CS gratings compared to the out-of-phase group. In contrast, synchronization did  
52 not amplify conditioned responding in physiological arousal (skin conductance) and  
53 visuocortical engagement (steady-state visually evoked potentials) during acquisition,  
54 although both measures demonstrated tuning towards the CS+. Together, these data support  
55 a causal role of theta-phase synchronization in affective evaluation and contingency report  
56 during fear acquisition.

57

## 58 Significance Statement

59 Due to methodological limitations, examining the causal role of oscillatory synchrony in  
60 association formation has been challenging so far. Using repetitive, rhythmic sensory  
61 stimulation in a memory-related 4 Hz frequency, we examined the role of phase  
62 synchronization in fear conditioning. While synchronization improved the contingency  
63 knowledge and affective evaluation, physiological arousal and visuocortical activity were  
64 unaffected by the phase-modulation. Our results represent an initial step towards  
65 establishing the causal effects of theta phase synchronization in associative fear learning,  
66 thus improving our understanding of the neurophysiological mechanisms of fear-memory  
67 encoding.

## 68 Introduction

69 Phase-synchronization of brain oscillations has been proposed as a mechanism supporting  
70 neuronal communication and plasticity (Fell & Axmacher, 2011). A theoretical perspective  
71 holds that the ongoing oscillatory phase reflects the excitability of a neural population and  
72 therefore determines a window for successful long-term-potential (LTP), a cellular process  
73 underlying learning and plasticity (Lynch, 2004). Research in rodents has shown that the  
74 induction of LTP or long-term depression (LTD) critically depends on oscillatory phases and  
75 the stimulation or recording site: While LTP was induced in behaving rats when the  
76 hippocampal CA1 was stimulated at the oscillatory peak, long-term depression (LTD)  
77 resulted from stimulation at the trough (Hyman et al., 2003). Using trace eyeblink  
78 conditioning in rabbits and recordings in the hippocampal fissure, CS-presentation in the  
79 trough induced phase-locked, regular (theta) oscillations that were in turn associated with  
80 better learning whereas CS-presentation to the peak impaired regularity and learning (Nokia  
81 et al., 2015). Note, that the theta phase reverses between the hippocampal fissure and the  
82 CA1 region. Since LTP requires precise timing between pre-and postsynaptic activation in  
83 the millisecond range (Markram et al., 1997), orchestrating activity by phase synchronization  
84 of neuronal oscillations is a potential mechanism supporting LTP. Among other oscillatory

phenomena, oscillations in the theta range (4-8 Hz in primates, 4-12 Hz in rodents) and their synchronization between memory-related brain sites are linked to memory performance (Headley & Paré, 2017). Rodent research (Benchenane et al., 2010; Place et al., 2016) and human EEG-studies (Summerfield & Mangels, 2005; Weiss & Rappelsberger, 2000) found increased theta synchronization between brain regions during different episodic memory tasks, suggesting that theta-synchronization facilitates communication (Fell & Axmacher, 2011).

Intriguingly, studies in humans have *causally* linked theta-phase synchronization to episodic associative memory. Repetitive, rhythmic sensory stimulation eliciting steady-state-evoked potentials (Clouter et al., 2017; Wang et al., 2018), enables experimental control over response frequency in a sensory region, and corresponding phase synchrony between regions (Hanslmayr et al., 2019; Herrmann et al., 2016; Thut et al., 2011). Synchronizing the oscillatory phase evoked by periodically modulated visual and auditory stimuli facilitated the encoding of an episodic audio-visual memory (Clouter et al., 2017; Wang et al., 2018), suggesting theta-phase synchronization as a mechanism for binding multisensory episodic memories. The synchronized input is assumed to increase temporally organized neuronal firing, which in turn may result in LTP (Buzsáki, 2002; Fries, 2015).

Although LTP is best understood in the hippocampus, its associative and synapse-specific properties make it a potential mechanism for plasticity in other regions (Bliss et al., 2018; Maren & Fanselow, 1995; Orsini & Maren, 2012). E.g., fear conditioning, a paradigm of associative emotional memory, involves associative plasticity within the lateral nucleus of the amygdala (Kim & Cho, 2017), but also in other structures processing the conditioned (CS) and unconditioned (US) stimuli (Herry & Johansen, 2014). Sensory information of both stimuli (typically different modalities) converge onto the same neuronal populations in the lateral amygdala (LA; Romanski et al., 1993). Activating weak CS synapses in temporal proximity to strong US synapses initiates a cascade of cellular reorganization, strengthening CS synapses and enabling the CS to elicit fear responses (Blair et al., 2001; Orsini & Maren, 2012). Importantly, theta synchronization between medial prefrontal cortex, amygdala, and

113 hippocampus plays a role during fear conditioning (Karalis et al., 2016; Seidenbecher et al.,  
114 2003; Taub et al., 2018; Zheng et al., 2019; for reviews see Bocchio et al., 2017; Çalışkan &  
115 Stork, 2018). However, its *causal* role in forming CS-US associations, is unknown.

116 The current study asked if synchronized sensory input helps the formation of a multisensory  
117 CS-US association in aversive learning. Using rhythmic external stimulation (cf., Clouter et  
118 al., 2017; Wang et al., 2018), we utilized “in-phase” vs. “out-of-phase” presentation of the  
119 visual CS and auditory US, in a 2-day fear conditioning using a generalization paradigm (5  
120 similar CS). We hypothesized that theta-band (4 Hz) synchronization of two distinct sensory  
121 systems promotes the CS-US association. Specifically, it was expected that in-phase  
122 presentation facilitates fear acquisition, whereas out-of-phase presentation prompts poor fear  
123 conditioning. Synchronizing the multisensory input is expected to orchestrate neuronal  
124 activity in the sensory cortices (so-called entrainment). If synchronization in the theta range  
125 provides a window for successful LTP, it should optimize conditions for synchronous afferent  
126 signals reaching further structures within the fear network, especially the lateral amygdala  
127 (LeDoux, 2000; Romanski et al., 1993). To assess different response systems in human fear  
128 conditioning, we measured conditioned responses in physiological arousal, affective  
129 evaluation of arousal and valence, contingency knowledge of CS and US, and visuocortical  
130 engagement.

131

## 132 **Materials and Methods**

### 133 *Participants*

134 The final sample comprised 40 healthy, right-handed students of the University of Osnabrück  
135 between 19 and 30 years ( $M = 22.2$ ,  $SEM = 0.35$ ; 20 men, 20 women). To control for sex-  
136 hormone fluctuations, female participants were only included if they used monophasic oral  
137 contraceptives (pill) and were examined between the 6<sup>th</sup> and 20<sup>th</sup> day of pill-intake (i.e., in the  
138 pill-on phase). Participants were screened via self-report questionnaire and a structured  
139 interview for inclusion and exclusion criteria in a screening session that was always  
140 conducted on a different day than the actual main experiment. Students with acute or chronic  
141 physical and/or psychiatric disorders (e.g., migraine, epilepsy, cardiovascular diseases and  
142 phobias) were not eligible. Further exclusion criteria encompassed hearing and/or  
143 uncorrected vision impairments, tinnitus, acute medication, drug abuse, average alcohol  
144 consumption exceeding 20 g or 40 g ethanol / day (for women and men, respectively), and  
145 smoking of > 5 cigarettes per day. Volunteers were screened for posttraumatic stress  
146 disorder (PTSD) using a translated version of the Posttraumatic Stress Diagnostic Scale  
147 (Foa, 2000; Steil & Ehlers, 2000) and excluded if they met the DSM-IV criteria for PTSD.  
148 From 64 volunteers (34 women), 46 (25 women) were eligible to participate, 3 women did not  
149 appear to the appointment and 3 (2 women) discontinued the main experiment due to the  
150 aversive nature of the conditioning paradigm, leading to our final sample of 40 participants.  
151 Within the female and male subsample, participants were randomly assigned to one of two  
152 groups: In-phase or out-of-phase, with the same number of men and women in each group  
153 (in-phase: 10 women; out-of-phase: 10 women).

154 The study was approved by the ethics committee of the University of Osnabrück and  
155 conducted in accordance with the Declaration of Helsinki guidelines. Written informed  
156 consent was obtained from all participants after adequate understanding of the explained  
157 procedures. Each participant was free to choose between participation credits (4 credits) or a

158 corresponding amount of money (32 €) for finishing screening and day 1 and 2 of our  
159 conditioning procedure.

#### 160 *Experimental design and stimuli*

161 We used a 2-day differential fear conditioning procedure, including habituation, acquisition,  
162 immediate extinction on day 1, and a 24-h delayed recall on day 2 (**Figure 1B**). Our study  
163 comprised a 5 x 2 mixed factorial design within each learning phase, with 5 CS-orientations  
164 of the below characterized Gabor-gratings (25°, 35°, 45°, 55°, and 65°) as the within-subject  
165 factor, and synchronization (in-phase, i.e., 0° phase shift vs. out-of-phase, i.e., 90°, 180°, and  
166 270° phase shift) as experimental between-subject factor.

167 Five high-contrast, black-and-white Gabor gratings (i.e., a sinusoid grating filtered with a  
168 Gauss-function) with a low spatial frequency served as the visual CS. The five CS differed  
169 only in orientation (25°, 35°, 45°, 55°, and 65°, relative to vertical 0°, **Figure 1A**). The CS  
170 were presented for 5 s centrally on a dark grey background (100% black setting on the  
171 monitor). During the presentation the experimental chamber was only lit by the CS on the  
172 screen. Technical failure forced us to exchange the monitor from a 19" (Acer P911) to a 17"  
173 (Sony, CPD-E220E) cathode ray tube (CRT) after examining the first 12 participants. We  
174 matched stimulus properties as closely as possible with the new monitor. The relevant  
175 parameters were comparable: i.e., 85 Hz refresh rate, low spatial frequency (0.96 vs. 0.81  
176 cycles/degree), large central CS presentation (5.70 vs. 5.73° visual angle), high contrast (96  
177 % Michelson for both monitors).

178 As the US, we employed a 2-s, broadband white noise (20 Hz – 22 kHz, 44100 Bit/s, 16  
179 Bits/sample), presented binaurally at a maximum of 96.5 dB(A) over two loudspeakers  
180 positioned 0.7 m left and right behind the participant. For an additional unimodal audio task  
181 (at the end of session on day 2) we presented the same white noise for 4 s at a non-aversive  
182 sound-pressure level with a maximum of 70.4 dB(A).

183 The intensity of the visual CS, the aversive auditory US and the non-aversive auditory noise  
184 (unimodal task) was modulated at 4 Hz (cf., Clouter et al., 2017). The luminance of the visual



CS was sinusoidally modulated in 4 Hz, where luminance changed at each screen refresh, resulting in 21 steps per cycle (0-100 % luminance). The amplitude of the auditory signal was sinusoidally modulated (0-100 %) in 4 Hz by multiplying the signal vector with a 4 Hz sine wave at the native 44.1 kHz audio sampling rate. Presentation of each 4-Hz modulated stimulus (auditory and visual) always started at 0 % intensity, increasing to 100% in the first half cycle.

--Insert Figure 1 here--

### *Conditioning procedure*

Our procedure included habituation, acquisition, and immediate extinction on day 1, as well as a 24-h delayed recall on day 2 (**Figure 1B**). During habituation, each 5-s, 4-Hz modulated CS was presented 12 times in pseudorandom order. Before acquisition, participants were instructed that only one of the 5 CS orientations will be followed by an aversively loud noise, without specifying which orientation. During the acquisition phase, each 4-Hz modulated CS was again presented 12 times. However, the 45° CS (CS+) was always paired (12 times) with the 2-s, 4-Hz modulated aversive noise US (reinforcement rate: 100%), while the other orientations were not (25°, 35°, 55°, and 65° gratings as CS-, **Figure 1B**). Previous work has used this same generalization paradigm, with 45° gratings serving as CS+, while also establishing that there are no systematic pre-conditioning differences between different grating orientations on the measures used here (McTeague et al., 2015). Previous work has also demonstrated that conditioning is seen across orientations and with counterbalancing (e.g., Moratti & Keil, 2005). Together, to facilitate interpretation and comparison with prior work, this led us to adopt a fixed contingency between 45° and the US. Each CS presentation was prolonged for the duration of the US, adding 2 s (i.e., 7-s duration for the CS+ and the CS- gratings during acquisition). For the 45° CS+, the last 2 s of visual CS overlapped with the auditory US presentation. Since retinal phototransduction was shown to be slower than auditory transduction (~ 50 ms for visual stimuli vs. 10 ms for auditory stimuli; King & Palmer, 1985; Lennie, 1981), the onset of the auditory US had a 40 ms delay relative

213 to the CS onset (cf. Clouter et al., 2017). The slower transduction of visual stimuli is also in  
 214 line with recordings in the amygdala after visual vs. auditory stimulation. The earliest activity  
 215 occurred between 40 and 80 ms (up to 316 ms, depending on the pathway to the amygdala  
 216 that differs in length) after visual stimulation (Luo et al., 2010; McFadyen et al., 2017;  
 217 Silverstein & Ingvar, 2015 for a review). In contrast, auditory information was recorded as  
 218 early as 10-40 ms in single-units of anesthetized as well as freely-moving rats (Quirk et al.,  
 219 1995; Romanski et al., 1993). This temporal difference in processing from receptors to the  
 220 afferent neurons in the CNS has to be considered when entraining the brain with  
 221 multisensory information in a synchronous way. Thus, adjusting for a temporal delay in one  
 222 modality is necessary to achieve theta synchronization of visual CS and auditory US in the  
 223 sensory cortices and facilitating synchrony of both input on the LA. CS presentation followed  
 224 one of two random sequences (Extended data Figure 1-1), with trial order constrained to not  
 225 allow more than two consecutive CS of the same orientation. Additionally, the acquisition  
 226 phase started with a booster sequence, where 5 of the first 7 trials were CS+US pairings.

227 The following immediate extinction, and the 24-h delayed recall phase comprised only CS  
 228 presentations (12 times each, no US), as in the habituation phase. The aversive US was not  
 229 presented at any point besides the 12 CS+US pairings in the acquisition phase. However,  
 230 neither before immediate extinction learning, nor before 24-h delayed recall, participants  
 231 were informed that no US will occur in the following stimulation phase.

232 Between the end of one CS presentation and the beginning of next one, a black screen was  
 233 shown for 3 to 5 s (random from a uniform distribution) during learning phases (1.5 to 3 s  
 234 during the unimodal audio task), followed by 1.5 s white fixation cross at the center of the  
 235 screen, resulting in an inter-trial-interval (ITI) between 4.5 and 6.5 s.

236 In accordance with Clouter et al. (2017), the 12 pairings of the 4-Hz modulated CS+ and US  
 237 were realized with either 0° (i.e., 0 ms) phase-shift (in-phase group), or in a 90° (62.5 ms),  
 238 180° (125 ms), and 270° (187.5 ms) shift for 4 USs each (out-of-phase group, **Figure 1C**).  
 239 Accounting for the 40-ms delay between rapid auditory and later visual processing times,

input with a phase-lag of  $0^\circ$  causes phase-synchronized cortical activity in the visual and auditory cortex (Clouter et al., 2017). This synchronized activity at the primary cortices is expected to increase the synchronized afferent signals reaching the amygdala, where CS-US convergence occurs, hence supporting associative plasticity in the lateral amygdala (Blair et al., 2001; Bocchio et al., 2017). In contrast, phase lags between  $90^\circ$  and  $270^\circ$ , i.e., timing shifts of 62.5-187.5 ms, should result in a suboptimal level of excitability and therefore decrease the likelihood of synaptic changes.

The experiment was conducted in an electromagnetically shielded and sound-attenuated experimental chamber, where participants were seated in a comfortable chair positioned centrally in front of the monitor. The experiment including all stimuli was created in MATLAB (2019b, RRID:SCR\_001622) using the Psychophysics Toolbox (RRID:SCR\_002881; Brainard, 1997; Kleiner et al., 2007).

#### *Sensory stimulation validation*

To validate the temporal fidelity of the stimulation, we analyzed data from two sources: a photo diode (Brain Products, Photo Sensor) attached to the participants' monitor, and a microphone (built into a BrainVision StimTrak) positioned in front of the participant's speakers. Both signals were recorded at 1000 Hz in BrainVision Recorder. The photo diode was placed over the upper right corner of the CRT monitor where a smaller version of the Gabor gratings appeared during the same monitor refresh cycle (and far outside of CS presentation area) in the same sinusoidal luminance modulation as the original CS-gratings. Pilot studies using photo sensors at both the upper corner (small test Gabor) and central screen (actual CS grating) showed excellent synchrony of both stimuli. The onset of the central grating was consistently 0.5 refresh cycles after the onset of the miniature grating in the top left corner, i.e.  $\sim 5.9$  ms. Using BrainVision Analyzer, data from the photo sensor and the microphone were segmented from -320 to 2500 ms relative to the onset of an US (i.e., 12 segments per subject), and visually inspected for artifacts. A subset of segments was

267 excluded, as microphone data were corrupted or missing due to failure of the StimTrack  
 268 batteries (in 5 out of 40 participants). For visualization, the remaining data were exported to  
 269 MATLAB and rescaled from  $-\pi$  to  $+\pi$ . Further analysis was computed over 7.02 cycles of  
 270 microphone and video data (1755 ms), disregarding the last cycle of audio stimulation. Video  
 271 data from -40 ms to +1715 ms relative to US onset were used. In contrast, microphone data  
 272 from 0 to 1755 ms entered analysis. This effectively shifts video data 40 ms forward in time,  
 273 to account for the 40 ms time shift programmed into the stimulus presentation. Microphone  
 274 data were first rectified (square root of the signal squared). Both, photo sensor and  
 275 microphone, channels were band-pass filtered between 3 and 5 Hz, using the *bandpass*  
 276 function of MATLAB's Signal Processing Toolbox with an IIR filter (60 dB attenuation at the  
 277 edge frequencies) and a steepness of .95. Instantaneous phase information at 4 Hz for audio  
 278 and video signal was extracted from the imaginary part of the analytic signal after a Hilbert  
 279 transform.

280 **--Insert Figure 2 here--**

281  
 282 This analysis also demonstrates that there was very little variability in the timing of sensory  
 283 stimulation within a trial, as well as between trials and between participants of one group.

#### 284 *Dependent variables*

285 ssVEPs (via EEG), skin conductance responses (SCRs), and subjective ratings served as  
 286 dependent outcomes. Further, horizontal and vertical eye movements were recorded by  
 287 electrooculography (EOG) with a bipolar BrainAmpExG amplifier (BrainProducts) to detect  
 288 and eliminate artifacts in the EEG-recordings.

#### 290 *EEG-parameters*

##### 291 *EEG-recording and pre-processing*

292 A 64-channel EEG was recorded on both days with two 32-channel BrainAmp DC amplifiers  
 293 with a resolution of 0.1  $\mu$ V (Brain Products). The 64 active electrodes (Ag/AgCl, actiCAP,

Brain Products) were filled with electrolyte gel (Super-Visc 10% NaCl, EasyCap) and positioned according to the extended international 10-20 system. Efforts were made to keep impedances below 5 k $\Omega$  (manufacturer's recommendation < 25 k $\Omega$ ). FCz served as recording reference and AFz as ground. A sampling rate of 1000 Hz and a high-pass filter at 0.016 Hz was used. In addition to the EEG, electrooculography was recorded with 4 Ag/AgCl electrodes ( $\varnothing$  4 mm) to control for eye movements: Two electrodes were placed on the lateral canthus of each eye for horizontal and two electrodes were placed infra- and supra-orbital, in line with pupil of the right eye, for vertical movements. An electrode on the forehead was attached as ground.

Offline pre-processing was done with Brain Vision Analyzer 2 software (version: 2.1.2.327). Raw data was band-pass filtered between 1 Hz and 100 Hz, using Butterworth (zero phase shift) filters with a 3dB low cutoff at 1 Hz (time constant: 0.1592, order 8) and a 3dB high cutoff at 100 Hz (order 4). Additional 50 and 100 Hz (1 Hz bandwidth, order 4) notch filters were applied to eliminate line noise. Data were segmented from -1250 to 7500 ms relative to a CS onset and an ocular correction independent component analysis (ICA), as implemented in BrainVision Analyzer, was applied. After visual inspection of the resulting factors and factor topographies, factors related to horizontal and vertical eye movements, blinks, as well as strong cardiac or muscular artefacts were removed from the reconstructed data. ICA-corrected data were re-referenced to an average reference, and the recording reference was re-included in the data as a 65<sup>th</sup> channel, at position FCz. The segments were cut to an interval between -1000 to 5000 ms relative to CS onset. With this segmentation, the US intervals were excluded from further analyses, to avoid contamination of our EEG-data. After another visual inspection, we rejected segments with remaining artefacts. On average, 3.93 segments were rejected per participant (0-15 rejected out of 240 segments for each participant). Data were down-sampled to 512 Hz, in accordance with Clouter et al. (2017) and exported to MATLAB (Mathworks, RRID:SCR\_00162). To increase spatial specificity, reduce volume conduction effects and to obtain reference-free data, we conducted a scalp current source density (CSD) transform (Junghöfer et al., 1997). The CSD values (as

estimates of cortical surface potentials) are represented on a sphere, approximating a cortical surface. For scalp-level analyses and topographical mapping, the CSD was projected back onto the original electrode space. Analyses were performed on CSD-transformed data, and CSD data are shown throughout the figures.

#### *Validation of visual and auditory entrainment (unimodal)*

To validate the visual cortical entrainment at 4 Hz, we first averaged CSD-transformed data over all habituation trials at each sensor of a participant in the time domain (disregarding CS-orientations, i.e. averaging 5 x 12 trials per subject). Habituation trials were not only strictly unimodal visual stimulation but precede any pairing of the CS with the aversive US. To avoid early ERP entering the frequency domain analysis, Fourier transform was applied on data from 750 to 5000 ms (i.e., containing 17 cycles of 4 Hz), post CS-onset. These data were windowed with a cosine-square window (20-point rise/fall) and subjected to a discrete Fourier transform (MATLAB) with a frequency resolution of 0.24 Hz. We extracted the absolute values of the Fourier coefficients at 4 Hz and transformed the resulting power values to signal-to-noise ratios (SNRs), using the average of 5 frequency bins under and 4 frequency bins above 4 Hz.

To validate auditory entrainment, we used the unimodal audio task at the end of day 2, as it reflected 4-Hz unimodal auditory stimulation, without concurrent visual stimulation. EEG-data from the audio-only task were subjected to the same pre-processing pipeline as CS-related data. As for visual unimodal data above, CSD-data were segmented (here from -1000 to 4100 ms, relative to audio stimulus onset) and averaged per participant and sensor over the 75 audio-only trials. Fourier transform was applied on windowed data (cosine-square, 20-point rise/fall) starting from 500 to 4000 ms after audio onset (i.e., containing 14 cycles of 4 Hz), resulting in a frequency resolution of 0.29 Hz. Like for the visual stimulation, we converted the power at 4 Hz to SNRs, using the average of the five frequency bins below and four above the frequency of interest as noise estimates.

349 **Figure 3** shows the scalp distribution of the 4-Hz SNR averaged over participants ( $N = 40$ ),  
 350 for the visual (**Figure 3A**) 4-Hz stimulation and the auditory 4-Hz stimulation (**Figure 3B**).  
 351 The average topographies are consistent with a typical visual and auditory steady-state  
 352 evoked potential at 4 Hz, respectively. Specifically, the relatively low driving frequency of 4  
 353 Hz has traditionally been shown to prompt larger spread of the ssVEP topography, reflective  
 354 of longer individual stimulation cycles, which allow spreading across the visual hierarchy  
 355 (e.g., Skrandies, 2007). However, the topographies of the 4-Hz EEG-signal showed some  
 356 variation between subjects. Therefore, for subsequent analyses in the frequency domain,  
 357 including single-trial analyses of CS-related activity, we selected the individual 6 sensors for  
 358 each participant showing the highest SNR at 4 Hz.

359 --Insert Figure 3 here--

#### 361 *ssVEP single-trial analysis*

362 We conducted a single-trial analysis to be able to show the temporal evolution of visual  
 363 cortical engagement over the course of learning trials. For single-trial analysis, we used data  
 364 segments between -1000 to 5000 ms, relative to CS-onset as 0 (in sample points at 512 Hz  
 365 sample rate, this is 1 to 3072 sample points with zero being sample point 512). First, we  
 366 sampled it up from 512 to 1536 Hz. Up-sampling the data ensured an integer number of  
 367 sampling points per one cycle for the 4 Hz as well as its harmonics (up to 16 Hz). At 1536  
 368 Hz, one cycle of the driving frequency (4 Hz) is 384 samples (instead of 128 at 512 Hz). By  
 369 subtracting the mean of the 1000 ms pre-stimulus interval, the data were baseline-corrected.  
 370 The power extraction of single trials was based on the analysis window between 750 and  
 371 5000 ms (relative to 0 ms = CS-onset). Over this analysis-window, a moving average  
 372 procedure was conducted. We obtained averages by shifting a window with a length of 4  
 373 cycles of the frequency of interest (i.e., 4 Hz) across the detrended data segments in steps of  
 374 one cycle and averaging the contents of the window with each step (12 steps, last 4-cycle  
 375 step starting at 3000 ms after CS-onset). We then transformed the single-trial estimates from  
 376 the time into the frequency domain using discrete Fourier transform (DFT) and extracted the



377 power at the driving frequency as the absolute of the Fourier coefficients, normalized by the  
378 length of FFT (here, 1536 sample points).

379 Interindividual variance in response strength and pre-experimental bias was corrected by  
380 calculating a *habituation ratio* for each CS (via division by habituation mean over all 60 trials  
381 of each participant, disregarding the different CS-orientation), with values larger than 1  
382 describing an enhancement and lower than 1 describing a decrease of ssVEP-power  
383 compared to habituation. In addition, single-trial data were smoothed with a moving average  
384 along the 12 trials (5-point symmetrical, shrinking at the endpoints) within each learning  
385 phase and CS-orientation (5 orientations x 4 learning phases with 12 trials each). For plots,  
386 showing the temporal evolution of ssVEP over trials we pooled data over sensors as the  
387 average of the individually defined six maximal SNR sensors for each participant. The  
388 individual sensors entering this 6-sensor cluster were defined as the 6 sensors showing the  
389 highest SNR at 4 Hz during habituation trials for a participant (see above, Validation of visual  
390 and auditory entrainment [unimodal]). Of note: while single-trial data is interesting and  
391 informative, we have no prior evidence allowing us to formulate specific hypotheses about  
392 group differences (in-phase vs. out-of-phase) in the temporal dynamics of ssVEP. Therefore,  
393 these data were averaged over all trials of a learning phase before statistical testing for  
394 group effects.

395

396 *Skin conductance responses (SCR) and electrocardiography (ECG), and blood pressure*  
397 *(BP)*

398 Besides ssVEP-power tunings towards specific CS-gratings, we used SCRs as a common  
399 measure of learning-induced changes in physiological arousal to the CS. However, as our  
400 lab is configured for stress-associated questions by default, we also recorded ECG and BP  
401 as control parameters only. ECG and BP will not be reported in the result section. We used a  
402 Brainamp ExG amplifier (Brain Products, Munich, Germany) and a 0.5 V constant voltage  
403 coupler to record SCRs with a sampling rate of 1000 Hz and a resolution of 0.0061  $\mu$ S. We



404 attached two Ø 10 mm (inner diameter) electrodes, filled with 0.05% NaCl paste (TD-246) on  
405 the thenar and hypothenar of the left hand (non-dominant) of each participant (Boucsein et  
406 al., 2012). No additional filters were applied. Data were down-sampled to 200 Hz in the  
407 BrainVision Analyzer 2.1 and exported to MATLAB. Responses with an onset latency  
408 between 1 and 4 s and a minimum amplitude of 0.02  $\mu$ S were automatically scored using  
409 Ledalab (Benedek & Kaernbach, 2010). If more than one response met the criteria, single  
410 responses were summed up. Responses that did not meet the criteria were scored as zero.  
411 After Ledalab scoring we used an additional visual inspection of heat maps of single trials  
412 and corrected 42 values (out of 240 trials x 40 participants = 9600 total values) that were  
413 over- or underscored by Ledalab. To further correct for interindividual differences and push  
414 distribution towards normal we calculated z-values, using the means and standard deviations  
415 (SD) over CS and US responses of all learning phases (habituation, acquisition, immediate  
416 extinction, and delayed recall) per participant. In accordance with ssVEPs, single-trial data  
417 were smoothed with a moving average along the 12 trials (5-point symmetrical, shrinking at  
418 the endpoints) within each learning phase and CS-orientation (5 orientations x 4 learning  
419 phases with 12 trials each). The z-standardized SCRs were then averaged across the 12  
420 trials of each learning phase and the averages were used in all statistical analyses.

421 For recording of ECG, we positioned three Ø 8 mm (inner diameter) electrodes (filled with  
422 5% NaCl ECG-paste, GE Medical Systems Information Technologies GmbH, Freiburg,  
423 Germany) under the right collarbone, the left shinbone, and (as ground electrode) on the  
424 right shinbone.

425 Systolic and diastolic BP were measured at discrete measurement points using a semi-  
426 automatic electronic sphygmomanometer (bosotron 2, Bosch + Sohn, Jungingen, Germany).  
427 Therefore, an inflatable cuff was placed around the left upper arm, with the sensor plate  
428 positioned over the brachial artery at heart level.

429

430 *Subjective ratings: Valence, arousal, and US-expectancy*

431 A paper-pencil version of the 9-point pictorial Self-Assessment Manikin (SAM) (Bradley &  
432 Lang, 1994) scale was used to evaluate each CS orientation for its valence (from negative to  
433 positive) and arousal (from excited to calm). Ratings were conducted after habituation,  
434 acquisition, immediate extinction as well as before and after 24-delayed recall. In addition,  
435 we asked the participants to rate their expectancy that an US occurs with the depicted  
436 grating with answers ranging from -5 (very certain, no) over 0 (uncertain) to 5 (very certain,  
437 yes). Except for after habituation, paper-pencil US-expectancy ratings were conducted  
438 together with our SAM ratings.

439

440 *Overall Procedure*

441 The study covered two parts: the screening session, lasting about one hour, explaining the  
442 general procedure of the main session, testing for inclusion and exclusion criteria and  
443 obtaining informed consent (see Participants section for description), and the main  
444 conditioning study. Screening and the main study were scheduled on different days.

445 *Main conditioning study:*

446 The main session was conducted on two consecutive days, starting at 10 am, 14 pm or  
447 17:30 pm. The duration of day 1 and day 2 of the main session were 2 hours and 1 hour,  
448 respectively. At the beginning of day 1 and day 2, we attached EEG, ECG, EOG, SCR  
449 electrodes and positioned the inflatable cuff for BP measures. Habituation, acquisition, and  
450 immediate extinction took place on day 1, while a 24-h delayed recall took place on day 2.  
451 After each learning phase on day 1 (i.e., after habituation, acquisition, extinction) as well as  
452 before and after delayed recall on day 2, resting periods, SAM and US expectancy ratings  
453 (except after habituation, where SAMs were conducted without US expectancy ratings, since  
454 no US has occurred), and ECG, SCR, as well as BP measures were done (see Fig. 1B).

455 Before starting the computer task, we read standardized “general information about the  
 456 experiment”, including a description of the procedure and the stimuli we were about to  
 457 present. Subjects were instructed to sit comfortably and avoid any movements (except eye  
 458 blinking) for the entire computer tasks and the explicitly announced measurement periods.  
 459 During the resting phases, subjects were encouraged to move carefully to avoid detachment  
 460 of electrodes. At the beginning of habituation, subjects were asked to fixate an upcoming  
 461 white cross in the center of the screen followed by some black and white ‘flickering’ gratings.  
 462 Prior to acquisition, we informed the participants that a loud ‘flickering’ noise would be  
 463 presented with only one of the gratings. However, we did not specify which of the five  
 464 orientations would predict the aversive noise. Prior to immediate extinction (day 1) and  
 465 delayed recall (day 2) participants were asked to remember the instructions, without  
 466 informing them that no aversive noise would be presented.

467

#### 468 *Statistical analysis*

469 We submitted each of the memory outcome measures (i.e., US-expectancy ratings, affective  
 470 valence and arousal ratings, SCRs, and ssVEPs) to a 5 x 2 repeated measures ANOVA,  
 471 conducted on SPSS software (SPSS 26.0 Inc, Chicago). The mixed ANOVA included the  
 472 within-subject factor orientation (i.e., the five CS: 25°, 35°, 45°, 55°, and 65°) and the  
 473 between-subject factor group (i.e., *in-phase* with 0° phase offset vs. *out-of-phase* with 90°,  
 474 180°, and 270° phase offset). To test for the expected form of the orientation effect  
 475 independent of group, we conducted a custom contrast for Generalization, using contrast  
 476 weights adapted from prior studies (**Figure 4 A**, Generalization weights: -0.529, 0.247,  
 477 0.564, 0.247, and -0.529).

478 As this is the first attempt to compare a synchronized vs. non-synchronized condition with a  
 479 fear generalization design, we hypothesized that group differences may manifest in one of  
 480 three possible ways: (1) Synchronized CS-US presentation may lead to major increases in  
 481 CS-responding not limited to the CS+ (this would be evident in a main effect group in the

ANOVA). (2) Synchronized CS-US presentation may dramatically change the pattern of responding over the five different CS (this could be evident in an orientation x group interaction in the ANOVA). (3) Finally, synchronized CS-US presentation may alter the width of the generalization curve. This could optimize learning, resulting in a narrower generalization and thus better discrimination between the five CS, without changing overall response levels or dramatically changing the response pattern. ANOVA interactions would not be able to detect this. Therefore, we designed a custom contrast for the group x orientation interaction, using the LMATRIX command for contrast coefficient matrices in SPSS. We obtained the contrast weights by subtracting a broader generalization profile (**Figure 4 B, orange line and font**) from a narrower generalization profile (**Figure 4 B, blue line and font**), resulting in a form resembling a 'Mexican Hat' (weights: 0.142, -0.489, 0.694, -0.489, and 0.142). We expected group differences to manifest during (or directly after) acquisition. However, to explore the longevity of potential group effects, we repeated our 5 x 2 ANOVA and the custom 'Mexican Hat' group x orientation contrast for extinction, and delayed recall on day 2.

--Insert Figure 4 here--

**Table 1.**

**Summary of statistical analyses.** Table shows statistical analyses including *p* value and effect size for each memory outcome measure, separated by learning phase. For each outcome measure, we calculated repeated-measures ANOVAs with the CS orientation as within-subject factor and the group (in-phase vs. out-of-phase) as between-subject factor. Successful conditioning, i.e., increased response towards the CS+ respective of group) was validated by main effects of orientations (noted in the column effects as **ME: o**). To account for the specific symmetric generalization pattern (CS+ in the middle), additional generalization contrast fits were used (noted as **GEN**). Main effects of group (**ME: g**) and group x orientation interactions (**o x g INT**) addressed differences between in-phase and out-of-phase conditioning. Better grating discrimination vs. stronger generalization across orientations are described by a Mexican Hat contrast fit for the group x orientation interactions (**MEX**).

	Data structure	Type of test	Effects	Statistic	p value	effect size
<b>US-expectancy</b>						
<i>Acquisition</i>						
a	normal	ANOVA	ME: o	$F_{(3,109)} = 12.491$	6.764E-7	$\eta^2_p = 0.247$
b	normal	ANOVA	GEN	$F_{(1,38)} = 28.360$	.000005	$\eta^2_p = 0.427$
c	normal	ANOVA	ME: g	$F_{(1,38)} = 7.310$	.010	$\eta^2_p = 0.161$
d	normal	ANOVA	o x g INT	$F_{(3,109)} = 1.133$	.338	$\eta^2_p = 0.029$
e	normal	ANOVA	MEX	$F_{(1,38)} = 4.796$	.035	$\eta^2_p = 0.112$
<i>Extinction</i>						
f	normal	ANOVA	ME: g	$F_{(1,38)} = 0.621$	.436	$\eta^2_p = 0.016$
g	normal	ANOVA	o x g INT	$F_{(3,113)} = 1.363$	.258	$\eta^2_p = 0.035$
h	normal	ANOVA	MEX	$F_{(1,38)} = 6.660$	.014	$\eta^2_p = 0.149$
<i>Delayed Recall (Day 2)</i>						
i	normal	ANOVA	ME: g	$F_{(1,36)} = 0.688$	.412	$\eta^2_p = 0.019$
j	normal	ANOVA	o x g INT	$F_{(3,100)} = 1.172$	.323	$\eta^2_p = 0.032$
k	normal	ANOVA	MEX	$F_{(1,36)} = 3.090$	.087	$\eta^2_p = 0.079$
<b>Valence &amp; Arousal</b>						
<i>Acquisition</i>						
l	normal	ANOVA <sub>Val</sub>	ME: o	$F_{(3,96)} = 7.756$	.000272	$\eta^2_p = 0.170$
m	normal	ANOVA <sub>Aro</sub>	ME: o	$F_{(3,100)} = 10.928$	.000008	$\eta^2_p = 0.223$
n	normal	ANOVA <sub>Val</sub>	GEN	$F_{(1,38)} = 12.354$	.001	$\eta^2_p = 0.245$
o	normal	ANOVA <sub>Aro</sub>	GEN	$F_{(1,38)} = 19.587$	.000078	$\eta^2_p = 0.340$
p	normal	ANOVA <sub>Val</sub>	ME: g	$F_{(1,38)} = 1.221$	.276	$\eta^2_p = 0.031$
q	normal	ANOVA <sub>Val</sub>	o x g INT	$F_{(3,96)} = 1.502$	.224	$\eta^2_p = 0.038$
r	normal	ANOVA <sub>Aro</sub>	ME: g	$F_{(1,38)} = 1.248$	.271	$\eta^2_p = 0.032$
s	normal	ANOVA <sub>Aro</sub>	o x g INT	$F_{(3,100)} = 1.658$	.187	$\eta^2_p = 0.042$
t	normal	ANOVA <sub>Val</sub>	MEX	$F_{(1,38)} = 9.228$	.004	$\eta^2_p = 0.195$
u	normal	ANOVA <sub>Aro</sub>	MEX	$F_{(1,38)} = 7.325$	.010	$\eta^2_p = 0.162$
<i>Extinction</i>						
v	normal	ANOVA <sub>Val</sub>	ME: g	$F_{(1,38)} = 1.810$	.186	$\eta^2_p = 0.045$
w	normal	ANOVA <sub>Val</sub>	o x g	$F_{(3,117)} = 0.647$	.590	$\eta^2_p = 0.017$

x	normal	ANOVA <sub>Aro</sub>	INT ME: g	$F_{(1,38)} = 0.355$	.555	$\eta^2_p = 0.009$
y	normal	ANOVA <sub>Aro</sub>	o x g INT	$F_{(3,112)} = 0.437$	.724	$\eta^2_p = 0.011$
<i>Delayed Recall (Day 2)</i>						
z	normal	ANOVA <sub>Val</sub>	ME: g	$F_{(1,36)} = 0.074$	.788	$\eta^2_p = 0.002$
aa	normal	ANOVA <sub>Val</sub>	o x g INT	$F_{(3,96)} = 0.216$	.864	$\eta^2_p = 0.006$
bb	normal	ANOVA <sub>Aro</sub>	ME: g	$F_{(1,36)} = 0.239$	.628	$\eta^2_p = 0.007$
cc	normal	ANOVA <sub>Aro</sub>	o x g INT	$F_{(3,100)} = .121$	.938	$\eta^2_p = 0.003$
<b>SCRs</b>						
<i>Acquisition</i>						
dd	normal	ANOVA	ME: o	$F_{(3,96)} = 14.856$	3.1057E-7	$\eta^2_p = 0.281$
ee	normal	ANOVA	GEN	$F_{(1,38)} = 31.987$	.000002	$\eta^2_p = 0.457$
ff	normal	ANOVA	ME: g	$F_{(1,38)} = 0.931$	.341	$\eta^2_p = 0.240$
gg	normal	ANOVA	o x g INT	$F_{(3,96)} = 0.833$	.461	$\eta^2_p = 0.021$
<i>Extinction</i>						
hh	normal	ANOVA	ME: g	$F_{(1,38)} = 1.170$	.286	$\eta^2_p = 0.030$
ii	normal	ANOVA	o x g INT	$F_{(3,117)} = 0.921$	.435	$\eta^2_p = 0.024$
<i>Delayed Recall (Day 2)</i>						
jj	normal	ANOVA	ME: g	$F_{(1,38)} = 0.002$	.965	$\eta^2_p = 0.00005$
kk	normal	ANOVA	o x g INT	$F_{(3,116)} = 1.483$	.222	$\eta^2_p = 0.038$
<b>ssVEPs</b>						
<i>Acquisition</i>						
ll	normal	ANOVA	ME: o	$F_{(4,137)} = 5.696$	.000479	$\eta^2_p = 0.130$
m	normal	ANOVA	GEN	$F_{(1,38)} = 8.447$	.006	$\eta^2_p = 0.182$
nn	normal	ANOVA	o x g INT	$F_{(4,137)} = 1.042$	.384	$\eta^2_p = 0.027$
<i>Extinction</i>						
oo	normal	ANOVA	ME: g	$F_{(1,38)} = 2.957$	.094	$\eta^2_p = 0.072$
pp	normal	ANOVA	o x g	$F_{(4,147)} = 0.418$	.790	$\eta^2_p = 0.011$

			INT			
<i>Delayed Recall (Day 2)</i>						
qq	normal	ANOVA	ME: g	$F_{(1,38)} = 5.354$	.026	$\eta^2_p = 0.123$
rr	normal	ANOVA	o x g INT	$F_{(3,122)} = 0.556$	.657	$\eta^2_p = 0.014$

Abbreviations: ANOVA = mixed repeated-measures ANOVA; ME = main effect;  
o=orientation;  $\eta^2_p$  = partial  $\eta^2$ ; g = group; MEX = Mexican Hat contrast fit of orientation x  
group interaction; INT = Interaction; GEN = Generalization fit; Val = Valence; Aro = Arousal

499

## 500 Results

501 *Phase synchronization causes a better discrimination between CS+ and neighboring CS-*  
502 *gratings in the US-expectancy ratings*

503 We found an effect of orientation on US-expectancies collected immediately after the CS+  
504 was repeatedly aversively reinforced during acquisition ( $F_{(3,109)} = 12.491$ ,  $p = 6.764\text{E-}7$ , part.  
505  $\eta^2 = .247$ ; **Table 1, a**). The resulting pattern reflected generalization around the CS+ (**Figure**  
506 **5**), with the CS+ and the most similar gratings receiving the highest US-expectancy scores  
507 (generalization contrast fit ( $F_{(1,38)} = 28.360$ ,  $p = .000005$ , part.  $\eta^2 = .427$ , **Table 1, b**). In  
508 addition, data revealed a main effect of group ( $F_{(1,38)} = 7.310$ ,  $p = .010$ , part.  $\eta^2 = .161$ ; **Table**  
509 **1, c**), but no group x orientation interaction (**Table 1, d**). Here, the out-of-phase group  
510 showed broader generalization of the US-expectancy ratings, while the in-phase group had a  
511 narrower generalization pattern with more discrimination between the CS+ and the four CS-  
512 (**Figure 5**). This was supported by a significant orientation x group interaction in the form of a  
513 Mexican Hat ( $F_{(1,38)} = 4.796$ ,  $p = .035$ , part.  $\eta^2 = .112$ ; **Table 1, e**). As a comprehensive index  
514 of CS discrimination (i.e., CS+ versus average of all CS-), we calculated *discrimination*  
515 *indices* by subtracting the weighted average of CS- responses from the CS+ responses  
516 (Extended data **Figure 5-1**). To account for the fact that the 35° and 55° CS- orientation only  
517 differ from the CS+ by 10° and are thus harder to discriminate, these orientations were  
518 multiplied with a weight of 0.33[...], before averaging. The more dissimilar orientations (25°,  
519 65°) differ by 20° from the CS+ and are easier to discriminate. Therefore, these two weighted

with 0.166[...], i.e., half of the weight of the more similar orientations. Although the CS- weights account for the perceptual difference, they are not directly derived from a psychophysics curve. **Figure 5-1** depicts estimation statistics for the discrimination indices within each learning phase by presenting individual values as well as the effect sizes (Hedge's  $g$ ) as a bootstrap 95% confidence interval (5000 samples) (Ho et al., 2019). To increase transparency, extended data, **Figure 5-2** shows the same for a discrimination index computed with the unweighted average of the four CS-.

For US-expectancy ratings collected after extinction, we found no main effect of group or a group x orientation interaction (**Table 1, f, g**). However, even after extinction trials the in-phase group showed a narrower generalization pattern than the out-of-phase group (**Figure 5**), Mexican Hat contrast fit for the orientation x group interaction: ( $F_{(1,38)} = 6.660$ ,  $p = .014$ , part.  $\eta^2 = .149$ , **Table 1, h**). On day 2, 24 h later (**Figure 5** and extended data **Figure 5-1**, day 2 before delayed recall) we found no group differences in US-expectancy ratings (no main effect group, no orientation x group interaction, **Table 1, i, j**), and the generalization was no longer significantly narrower in the in-phase group (Mexican Hat orientation x group interaction, **Table 1, k**).

--Insert Figure 5 here--

*Synchronization leads to a narrower rating pattern towards the CS+ in valence and arousal ratings after fear acquisition*

For both, valence and arousal ratings after acquisition (**Figure 6**), we found a similar prioritization of the CS+ as for US-expectancy (main effect orientation; valence:  $F_{(3,96)} = 7.756$ ,  $p = .000272$ , part.  $\eta^2 = .170$ , **Table 1, l**; arousal:  $F_{(3,100)} = 10.928$ ,  $p = .000008$ , part.  $\eta^2 = .223$ , **Table 1, m**). Again, reflecting generalization around the CS+ (Generalization fit: valence:  $F_{(1,38)} = 12.352$ ,  $p = .001$ , part.  $\eta^2 = .245$ , **Table 1, n**; arousal:  $F_{(1,38)} = 19.587$ ,  $p = .000078$ , part.  $\eta^2 = .340$ , **Table 1, o**). Here, mixed ANOVA showed no group main effect or orientation x group interaction for valence (**Table 1, p, q**) and arousal (**Table 1, r, s**).



547 However, in both measures the in-phase group showed a narrower generalization than the  
 548 out-of-phase group (**Figure 6**). This was evident in significant orientation x group interactions  
 549 in the form of a Mexican Hat for valence ( $F_{(1,38)} = 9.228$ ,  $p = .004$ , part.  $\eta^2 = .195$ , **Table 1, t**)  
 550 and arousal ( $F_{(1,38)} = 7.325$ ,  $p = .010$ , part.  $\eta^2 = .162$ , **Table 1, u**). The discrimination indices  
 551 (CS+ versus averaged CS-) as well as estimation plots including individual values and effect  
 552 sizes are additionally presented in **Figure 6-1**.

553 After extinction, there were no effects of synchronization in valence (group main effect or  
 554 orientation by group interaction **Table 1, v, w**) or arousal (group main effect or orientation by  
 555 group interaction **Table 1, x, y**). The same was true for valence and arousal ratings on day 2  
 556 (group main effect and orientation x group interaction, valence: **Table 1, z, aa**; arousal:  
 557 **Table 1, bb, cc**).

558 **--Insert Figure 6 here--**

559  
 560 *SCRs showed the typical increase towards the reinforced CS+ but were unaffected by the*  
 561 *synchronization conditions*

562 **Figure 7A, B** depicts the SCRs on a trial by trial basis, to visualize temporal dynamics of  
 563 moving-averaged and z-transformed SCRs. In addition, z-values (i.e., without moving-  
 564 average) SCRs are presented in **Figure 7-1**. However, as single trials are subject to noise,  
 565 SCRs were analyzed using averaged data (**Figure 7 C**) as described in the method section.  
 566 Pairing the CS+ orientation with the aversive US within acquisition, led to the predicted  
 567 increase of SCR towards the reinforced grating (main effect orientation;  $F_{(3,96)} = 14.856$ ,  $p =$   
 568  $3.1057\text{E-}7$ , part.  $\eta^2 = .281$ , **Table 1, dd**). The response pattern was described by  
 569 generalization around the CS+ (Generalization fit:  $F_{(1,38)} = 31.987$ ,  $p = .000002$ , part.  $\eta^2 =$   
 570  $.457$ , **Table 1, ee**). However, this was independent of group (main effect group and  
 571 orientation x group interaction, **Table 1, ff, gg**, see **Figure 7-2** for discrimination indices and  
 572 estimation statistics). Looking at Figure 7 (and Extended Data Figure 7-1), it is unusual that  
 573 SCRs towards the CS+ seem already increased on the very first trial of acquisition,

independent of the applied smoothing procedure (see Extended Data Figure 7-1 for unsmoothed data). However, explorative analyses of group differences without the first trial did not change the results, i.e., there was still no overall difference between groups and no significant orientation x group interaction.

During *extinction*, there was no difference between groups (main effect group and orientation x group interaction, **Table 1, hh, ii**) and also on day 2 synchronization had no effects (main effect group and orientation x group interaction, **Table 1, jj, kk**).

--Insert Figure 7 here--

*ssVEP-power revealed a tuning towards the visual CS+ that was similar in both groups*

**Figure 8 A, B** depicts ssVEPs on trial-by-trial basis, to visualize temporal dynamics and the Extended Data **Figure 8-1** shows ssVEP-ratios without moving-average. However, as for the SCRs, ssVEPs were analyzed using averaged data (**Figure 8 C**) as described in the method section.

ssVEPs during acquisition revealed a conditioned power increase towards the CS+ and neighboring gratings (main effect orientation,  $F_{(4,137)} = 5.696$ ,  $p = .000479$ , part.  $\eta^2 = .130$ , **Table 1, ll**). It was described by a generalization pattern around the CS+ (Generalization fit,  $F_{(1,38)} = 8.447$ ,  $p = .006$ , part.  $\eta^2 = .182$ , **Table 1, mm**). However, this prioritization was not affected by group (orientation x group interaction, **Table 1, nn**). In similarity to SCRs during acquisition, Figure 8 A and B indicate an increased ssVEP ratio towards the CS+ on the very first trial. However, considering the unsmoothed data in Extended Data Figure 8-1, the power increase here seems to be an artifact of the applied smoothing procedure. As depicted in **Figure 8 C**, synchronization had also no effects on ssVEPs in *extinction*. Consequently, we neither found a significant main effect of group nor an orientation x group interaction (**Table 1, oo, pp**). Intriguingly, the ssVEP-power during delayed recall on day 2 was generally higher in the in-phase group than in the out-of-phase group ( $F_{(1,38)} = 5.354$ ,  $p = .026$ , part.  $\eta^2 = .123$ , **Table 1, qq**), although this effect was independent of orientation (orientation x group

601 interaction, **Table 1, rr**) (**Figure 8, c**). In accordance with ratings and the SCRs,  
602 discrimination indices (weighted CS+ minus averaged CS- gratings) and estimation plots,  
603 depicting individual values and effects sizes are presented in **Extended Data Figure 8-2**.

604 --Insert Figure 8 here--

605

606

## 607 **Discussion**

608 The formation of associative memories is an elemental aspect of human behavior, but its  
609 underlying neurocomputations are largely unknown. One group of theoretical notions has  
610 emphasized the role of phase-synchronized oscillations for binding representations of  
611 conditioned cues to behavioral outcomes (e.g., Headley & Paré, 2017). Recent research has  
612 increasingly utilized external rhythmic stimulation to test the role of phase relations in specific  
613 frequency bands for the formation of working memory (Polanía et al., 2012; Violante et al.,  
614 2017) and audiovisual associations (Clouter et al., 2017; Wang et al., 2018). Based on these  
615 previous findings, we applied this method for the first time in a fear conditioning paradigm.  
616 Modulating the phase-shift of a visual CS and aversive auditory US that was presented in the  
617 memory-relevant theta frequency allowed us to causally interpret phase synchronization in  
618 fear conditioning. To assess the various response systems that are important in fear learning  
619 (Lang et al., 2000), we measured skin conductance responses, indexing the physiological  
620 arousal of fear, ratings of valence and arousal to capture the subjective evaluation of each  
621 stimulus, and US-expectancies which assesses the participant's knowledge of the CS-US  
622 association. Additionally, ssVEPs provided information about visuocortical engagement and  
623 tuning patterns in sensory processing.

624 The measures we collected in the current study reflect different facets of the associative  
625 conditioning process and as such responded differently to the experimental manipulations. In  
626 accordance with our hypothesis, synchronized CS-US presentation facilitated the ability to  
627 identify the CS+ as the grating that was most likely followed by the aversive US. Remarkably,  
628 participants that received synchronized CS-US presentation discriminated the CS+ more  
629 precisely from the neighboring CS- gratings (which only differed in an orientation shift of 10°).  
630 Participants in the out-of-phase group, in contrast, generalized across the CS+ or the most  
631 similar CS- gratings. We therefore conclude that the synchronous input of two (multimodal)  
632 stimuli stemming from two sensory modalities strengthens the cognitive representation of the  
633 CS-US association.

634 Consistent with the US-expectancies, the subjective valence and arousal ratings reflected  
635 the effects of phase synchronization: While participants who received in-phase stimulation  
636 were more sensitive to changes in the perceived valence and arousal of the CS+,  
637 participants in the out-of-phase group reported generalized arousal and unpleasantness  
638 across the CS+ and neighboring CS- gratings. Hence, synchronous input not only sharpens  
639 the cognitive representation of CS-US contingency but seems to have a similar influence on  
640 the affective evaluation.

641 Surprisingly, there were no corresponding effects in the SCR or ssVEP data. Considering  
642 SCR data, during acquisition both groups showed the strongest response towards the CS+  
643 grating, independent of synchronization. Especially in the single-trial data, however, the in-  
644 phase group appears to respond stronger towards the CS+, which seems to be more  
645 pronounced in the first trials. We therefore exploratively tested the potential group difference  
646 by segmenting the trials into trial blocks (3 blocks with 4 trials per block). However, adding  
647 this within-factor to our statistical analysis did not reveal any significant differences between  
648 the groups in different phases of acquisition. One possible explanation of the higher SCRs in  
649 the beginning of acquisition might be the utilized booster sequence (i.e., 5 of the first 7  
650 gratings were CS+ gratings). The booster and the applied criterium to not allow more than  
651 two consecutive CS of the same orientation might also be the reason for another unusual  
652 observation within our SCR results: Irrespective of the factor group and independent of the  
653 applied smoothing procedure, SCR towards the CS+ was already increased on the very first  
654 trial. While we applied the booster sequence for a better comparability with previous findings  
655 (Antov et al., 2020; McTeague et al., 2015), future studies should consider a different  
656 approach to minimize similar trial order effect. Nevertheless, there was no differences  
657 between the in-phase and out-of-phase group, thus this observation does not change the  
658 following interpretations.

659 An effect of phase synchronization was also missing in the ssVEP-data: Although we were  
660 able to detect a tuning pattern with the greatest power for the reinforced CS+ grating for 4-Hz

661 stimulus presentation as previously described for stimulation in the low beta-range (Antov et  
662 al., 2020; McTeague et al., 2015), the pattern did not differ between in-phase and out-of-  
663 phase group.

664 A possible explanation for the observed discrepancies in the different variables could be the  
665 involvement of different memory types we might have assessed with our measures. Although  
666 fear conditioning is a well-established and widely used paradigm, it is difficult to strictly  
667 distinguish the mechanisms behind each response system. For example, skin conductance  
668 responses measure physiological arousal during fear learning (although it is not restricted to  
669 fear conditioning) and is often considered as measure of the unaware fear reaction,  
670 especially dependent on the amygdala (Christopoulos et al., 2019; Knight et al., 2003, 2006;  
671 but see also Lovibond & Shanks, 2002; Sevenster et al., 2014). US-expectancy ratings, on  
672 the contrary, are considered to specifically reflect declarative knowledge of the CS-US  
673 contingency (Boddez et al., 2013), which is known to include additional brain structures like  
674 the hippocampus. Bechara et al. (1995) observed a neural dissociation between implicit and  
675 explicit aspects of a fear conditioning procedure. While patients with bilateral amygdala  
676 lesions were unable to elicit SCRs but had an intact memory for the declarative facts,  
677 patients with bilateral lesions of the hippocampus showed the exact opposite effects, i.e.,  
678 they acquired SCRs but failed to recall declarative facts. Speculating that the effects of  
679 visual-auditory stimulation is not only restricted to early sensory cortices, but influences  
680 deeper brain regions in the course of rhythmic processing, our results might be explainable  
681 based on these distinct systems: theta phase synchronization might especially modulate the  
682 path involved in forming declarative facts about the CS-US pairing (i.e., US-expectancy  
683 ratings), probably including the hippocampus, without influencing the emotional conditioning  
684 comprising the amygdala. One possible mechanism could be that the phase-synchronous  
685 visual CS+ and auditory US simultaneously arrives at neural populations in the hippocampus,  
686 increasing the likelihood of long-term potentiation and thereby enhancing synaptic strength  
687 (Fell & Axmacher, 2011). Although the EEG method used here does not allow drawing  
688 conclusions about mechanisms at the synaptic level in subcortical structures, one might also

689 speculate why the heightened CS-US association in the rating data is not reflected in metrics  
 690 thought to reflect limbic processing, i.e., the SCRs. There are two potential explanations that  
 691 we wish to highlight in this context: 1) In various species, theta-phase synchronization has  
 692 predominantly been examined in the context of LTP in the hippocampus (e.g., Buzsáki, 2002;  
 693 Huerta & Lisman, 1995; Hyman et al., 2003; Lega et al., 2012), which is specifically relevant  
 694 in the formation of declarative memory (Clouter et al., 2017; Eichenbaum, 1999; Wang et al.,  
 695 2018). Thus, one may speculate that theta-phase synchronization is linked to hippocampus-  
 696 dependent processes, whereas the exact timing of CS and US may play a lesser role in  
 697 amygdala-dependent fear learning. However, some studies have found theta-phase  
 698 synchronization between the amygdala and other important structures of the fear circuit (e.g.,  
 699 hippocampus, ventrolateral PFC, anterior gyrus cinguli) as well as within the subnuclei of the  
 700 amygdala (Karalis et al., 2016; Seidenbecher et al., 2003; Taub et al., 2018; Zheng et al.,  
 701 2019; for reviews see Bocchio et al., 2017; Çalışkan & Stork, 2018) during different stages of  
 702 the fear conditioning process, supporting the general influence of theta synchronization  
 703 during fear memory formation. As such, future work may wish to characterize the role of  
 704 synchronization within and between specific brain regions for the establishing and  
 705 maintenance of fear memories. 2) More importantly, however, is the question if synchronized  
 706 theta rhythms propagate to the amygdala. Sensory information reaches the amygdala via  
 707 multiple pathways among which some are faster and sub-cortical or “low” route and others  
 708 are slower or “high” cortical routes (Silverstein & Ingvar, 2015). Since our method of visual  
 709 and auditory synchronized (vs. asynchronized) theta stimulation is delivered globally and is  
 710 unlikely to target one specific pathway, the timing might not have been suitable to enable  
 711 locally specific synchronization. Considering that we used a generalization paradigm with  
 712 similar CS gratings, we may offer the speculation that the challenging discrimination of the  
 713 CS+ requires a more demanding processing via the slow, cortical route, while the simple  
 714 aversive US reaches the amygdala via the fast, subcortical pathway. Thus, the 40 ms we  
 715 added to the US might have been insufficient to achieve theta-synchronization when the CS  
 716 and US reaches the LA. Due to the relatively long CS-US overlap of 2 seconds, we

717 additionally cannot rule out that our synchronized stimulation reached the amygdala via the  
718 thalamic route first, but then also via cortical routes, leading to cancellation of the first CS-US  
719 phase synchronization, hence minimizing the suggested effects.

720 Another interesting consideration in this context is the role of theta synchronization between  
721 the amygdala and hippocampus for pattern separation of emotional images: Examining pre-  
722 surgical epilepsy patients, Zheng et al. (2019) found that bidirectional theta synchronization  
723 between both structures was associated with the ability to discriminate an encoded image  
724 and a new, but similar 'lure' image in a test phase. Considering that most of our results  
725 consists in a better discrimination between the aversive CS+ and the most similar CS-  
726 gratings, synchronized CS-US presentation might be beneficial for the amygdalo-  
727 hippocampal communication, associated with enhanced discrimination of emotional content.  
728 However, further research with additional outcome measures is needed to pinpoint all  
729 underlying neurophysiological processes. For example, future studies may attempt to  
730 experimentally untangle declarative and non-declarative memory processes involved in fear  
731 conditioning, including their reactivity to synchronized presentation. Measuring amygdala and  
732 hippocampal activity via fMRI or in experimental animals may also help to clarify the  
733 influence of synchronized presentation on distinct sub-processes of fear conditioning and  
734 their associated neural substrates.

735 One important consideration when interpreting the current results is the fact that group  
736 differences were mostly restricted to the encoding phase of fear (acquisition), although we  
737 expected that improved fear learning after synchronous presentation prompts greater  
738 extinction resistance. Contrary to expectations, we did not find extinction-resistant patterns in  
739 the in-phase group during immediate extinction or delayed recall. However, using a  
740 reinforcement rate of 100% is known to cause rapid extinction (e.g., Dunsmoor et al., 2007;  
741 Haselgrove et al., 2004), which could make it harder to detect between-group effects.  
742 Moreover, because extinction leads to the formation of a new (i.e., CS-noUS) memory trace  
743 that inhibits the original fear memory, future research may wish to employ a second CS+



744 stimulus that is not extinguished, which will aid in assessing the long-lasting effects of theta-  
745 phase synchronization on fear memory recall (i.e., the trace that was causally manipulated  
746 by theta-synchronized stimulation). Additionally, animal and human work suggests that  
747 prolonged stimulus-free periods during encoding are associated with the more effective  
748 production of long-term memory (Jiang et al., 2020; Philips et al., 2013). Increasing the inter-  
749 trial-intervals (ITI) might help to form more robust memory traces that persist over time.  
750 Another possible cause for the absence of long-term effects of stimulation phase is that the  
751 externally modulated CS-US stimulation only affects short-term or working memory  
752 processes but does not have any effects on actual long-term memory. In two comparable  
753 studies focusing on working memory, Clouter et al. (2017) and their follow-up study by Wang  
754 et al. (2018) used a distractor task as a time gap between encoding and recall of the learned  
755 video-tone associations, which only lasted for 30 seconds, likely too short to inform the  
756 formation of long-term memory.

757 Although the current study provided evidence of a causal role of theta-phase synchronization  
758 in the context of fear conditioning, there are some limitations to consider. First, our sample  
759 size was chosen to detect medium to strong effect sizes, which was based on previous  
760 studies (Clouter et al., 2017; Wang et al., 2018). Therefore, we cannot rule out the possibility  
761 that we could not detect small effect sizes. This is especially interesting for the SCR data,  
762 where the responses are descriptively stronger after in-phase CS-US presentation, but the  
763 statistics did not show significant differences. Increasing the statistical power via a greater  
764 sample size might help to even detect small effect sizes.–Second, we cannot conclude that  
765 the stimulation effects observed here are specific to the theta band, because we did not test  
766 other frequencies. However, both animal model studies that examined theta-phase  
767 synchronization in the fear network (e.g., Seidenbecher et al., 2003; Taub et al., 2018), as  
768 well as entrainment studies that focused on working and declarative memory (e.g.,  
769 Alekseichuk et al., 2016; Clouter et al., 2017; Violante et al., 2017) support the current  
770 conclusion that synchronization in the theta-frequency band is specifically important for fear  
771 memory formation. Third, we did not explicitly ask whether participants were able to detect

772 the synchronous or asynchronous timing between CS and US, and therefore we cannot rule  
 773 out that out-of-phase or in-phase stimulation exerted effects based on phenomenological,  
 774 perceptual differences. Nevertheless, we used the exact time lags utilized by both, Clouter et  
 775 al. (2017) as well as Wang et al. (2018) who did not observe any interference with perceptual  
 776 judgments or decline in performance. In addition, Clouter et al. (2017) conducted a control  
 777 experiment with static stimuli which, on a perceptual basis, represents the best-case  
 778 scenario for perceptual binding and still found better results after theta-synchronized video-  
 779 audio presentation. Fourth, although EEG data showed a group-independent tuning towards  
 780 the CS+ grating, supporting the conditioned effects on sensory processing, the hypothesized  
 781 sharpening in the in-phase group was not confirmed. What we found is a general increase in  
 782 ssVEP-power in the in-phase group during day 2, suggesting a stronger engagement of the  
 783 sensory cortex. However, based on the present data, we cannot establish to what extent this  
 784 effect was caused by the theta-phase synchronization on day 1 as opposed to arising as an  
 785 epiphenomenon, e.g., of the cognitive changes induced by the synchronization. Fifth, theta-  
 786 synchronization may not facilitate learning, but desynchronized stimulation may disrupt  
 787 ongoing oscillatory processes, resulting in less precise (i.e., more generalized) fear  
 788 responses (Alekseichuk et al., 2017). To clarify this assumption, future work may include a  
 789 third group in which participants are presented with non-flickering CS and US stimuli.

790 Finally, an important limitation is that we were not able to show that participants' auditory and  
 791 visual EEG responses were synchronized or de-synchronized as intended. This was due to  
 792 limited number of trials and noisy US-data. In contrast to previous work with innocuous  
 793 stimuli, the US in a fear conditioning experiment has to be highly aversive. Inherently, this  
 794 means that the duration of the US (the only period where auditory and visual stimulation  
 795 overlap) will produce noisy EEG-data with many movement, startle-response, and other  
 796 artifacts. This is why EEG studies of human fear conditioning (regardless of the US used and  
 797 of the of number trials) typically do not analyze any data during US-presentation window.  
 798 Because the US is aversive, we did not want to expose participants to more noise than  
 799 absolutely necessary. Thus, based on previous experiments, we limited the duration of a

800 single US to 2000 ms and the US trials to 12 per participant. In combination with inherently  
801 noisy EEG-data during a US-presentation precluded us from localizing and analyzing phase  
802 differences in the brain response. This should be addressed with a modified design in future  
803 studies. Nevertheless, we did verify the precise nature of the bi-modal stimulation on a  
804 single-trial and single-subject level (Figure 2). Importantly, earlier work (Clouter et al., 2017;  
805 Wang et al., 2018) with 4-Hz audio-video synchronization using larger trial numbers and non-  
806 aversive audio stimulation have shown that precise audio-video stimulation results in  
807 synchronized responding in the auditory and visual cortex. Future studies may also consider  
808 extending the temporal gap between the acquisition phase and the delayed recall, because  
809 previous work has indicated that theta-band synchronization between the amygdala and  
810 sensory cortices affects the storage of fear information in remote, but not recent fear retrieval  
811 (Do-Monte et al., 2015; Sacco & Sacchetti, 2010).

812 In conclusion, the current study represents an initial step towards establishing the causal  
813 effects of theta-phase synchronization for fear memory formation. Our results replicate the  
814 importance of synchronization for acquiring new cognitive representations, measured via US-  
815 expectancy ratings, and affective evaluation (subjective valence and arousal ratings). By  
816 contrast, the present evidence was mixed at the level of sympathetic (skin conductance) and  
817 visuocortical (ssVEPs) engagement. Future studies may wish to further explore the  
818 differentiation between different response systems in the context of fear conditioning.  
819 Leveraging the potential of rhythmic stimulation and synchronization while taking into  
820 account the evolution of fear acquisition across the learning phases will ultimately assist in  
821 improving our understanding of the mechanisms behind the acquisition of learned fear  
822 responses.

823

824 **References**

- 825 Alekseichuk, I., Pabel, S. C., Antal, A., & Paulus, W. (2017). Intrahemispheric theta rhythm  
 826 desynchronization impairs working memory. *Restorative Neurology and Neuroscience*,  
 827 35(2), 147–158. <https://doi.org/10.3233/RNN-160714>
- 828 Alekseichuk, I., Turi, Z., Amador de Lara, G., Antal, A., & Paulus, W. (2016). Spatial working  
 829 memory in humans depends on theta and high gamma synchronization in the prefrontal  
 830 cortex. *Current Biology*, 26(12), 1513–1521. <https://doi.org/10.1016/j.cub.2016.04.035>
- 831 Antov, M. I., Plog, E., Bierwirth, P., Keil, A., & Stockhorst, U. (2020). Visuocortical tuning to a  
 832 threat-related feature persists after extinction and consolidation of conditioned fear.  
 833 *Scientific Reports*, 10(1), 3926. <https://doi.org/10.1038/s41598-020-60597-z>
- 834 Bechara, A., Tranel, D., Damasio, H., Adolphs, R., Rockland, C., & Damasio, A. (1995).  
 835 Double dissociation of conditioning and declarative knowledge relative to the amygdala  
 836 and hippocampus in humans. *Science*, 269(5227), 1115–1118.  
 837 <https://doi.org/10.1126/science.7652558>
- 838 Benchenane, K., Peyrache, A., Khamassi, M., Tierney, P. L., Gioanni, Y., Battaglia, F. P., &  
 839 Wiener, S. I. (2010). Coherent theta oscillations and reorganization of spike timing in the  
 840 hippocampal- prefrontal network upon learning. *Neuron*, 66(6), 921–936.  
 841 <https://doi.org/10.1016/j.neuron.2010.05.013>
- 842 Benedek, M., & Kaernbach, C. (2010). A continuous measure of phasic electrodermal  
 843 activity. *Journal of Neuroscience Methods*, 190(1), 80–91.  
 844 <https://doi.org/10.1016/j.jneumeth.2010.04.028>
- 845 Blair, H. T., Schafe, G. E., Bauer, E. P., Blair, H. T., Schafe, G. E., Bauer, E. P., Rodrigues,  
 846 S. M., & Ledoux, J. E. (2001). Synaptic plasticity in the lateral amygdala: a cellular  
 847 hypothesis of fear conditioning. *Learning & Memory*, 8, 229–242.  
 848 <https://doi.org/10.1101/lm.30901>
- 849 Bliss, T. V. P., Collingridge, G. L., Morris, R. G. M., & Reymann, K. G. (2018). Long-term  
 850 potentiation in the hippocampus : discovery, mechanisms and function. *Neuroforum*,  
 851 24(3), 103–120.
- 852 Bocchio, M., Nabavi, S., & Capogna, M. (2017). Synaptic plasticity, engrams, and network  
 853 oscillations in amygdala circuits for storage and retrieval of emotional memories.  
 854 *Neuron*, 94(4), 731–743. <https://doi.org/10.1016/j.neuron.2017.03.022>
- 855 Boddez, Y., Baeyens, F., Luyten, L., Vansteenwegen, D., Hermans, D., & Beckers, T. (2013).  
 856 Rating data are underrated: Validity of US expectancy in human fear conditioning.  
 857 *Journal of Behavior Therapy and Experimental Psychiatry*, 44(2), 201–206.  
 858 <https://doi.org/10.1016/j.jbtep.2012.08.003>
- 859 Boucsein, W., Fowles, D. C., Grimnes, S., Ben-Shakhar, G., Roth, W. T., Dawson, M. E., &  
 860 Fillion, D. L. (2012). Publication recommendations for electrodermal measurements.  
 861 *Psychophysiology*, 49(8), 1017–1034. <https://doi.org/10.1111/j.1469-8986.2012.01384.x>
- 862 Bradley, M. M., & Lang, P. J. (1994). Measuring emotion: the Self-Assessment Manikin and  
 863 the Semantic Differential. *Journal of Behavior Therapy and Experimental Psychiatry*,  
 864 25(1), 49–59. <http://www.ncbi.nlm.nih.gov/pubmed/7962581>
- 865 Brainard, D. H. (1997). The Psychophysics Toolbox. *Spatial Vision*, 10(4), 433–436.  
 866 <https://doi.org/10.1163/156856897X00357>
- 867 Buzsáki, G. (2002). Theta oscillations in the hippocampus. *Neuron*, 33, 1–16.
- 868 Çalışkan, G., & Stork, O. (2018). Hippocampal network oscillations as mediators of

- behavioural metaplasticity: Insights from emotional learning. *Neurobiology of Learning and Memory*, February. <https://doi.org/10.1016/j.nlm.2018.02.022>
- Christopoulos, G. I., Uy, M. A., & Yap, W. J. (2019). The body and the brain: measuring skin conductance responses to understand the emotional experience. *Organizational Research Methods*, 22(1), 394–420. <https://doi.org/10.1177/1094428116681073>
- Clouter, A., Shapiro, K. L., & Hanslmayr, S. (2017). Theta phase synchronization is the glue that binds human associative memory. *Current Biology*, 27(20), 3143–3148.e6. <https://doi.org/10.1016/j.cub.2017.09.001>
- Do-Monte, F. H., Quinões-Laracuenta, K., & Quirk, G. J. (2015). A temporal shift in the circuits mediating retrieval of fear memory. *Nature*, 519(7544), 460–463. <https://doi.org/10.1038/nature14030>
- Dunsmoor, J. E., Bandettini, P. A., & Knight, D. C. (2007). Impact of continuous versus intermittent CS-UCS pairing on human brain activation during Pavlovian fear conditioning. *Behavioral Neuroscience*, 121(4), 635–642. <https://doi.org/10.1037/0735-7044.121.4.635>
- Eichenbaum, H. (1999). The hippocampus and mechanisms of declarative memory. *Behavioural Brain Research*, 103(2), 123–133. [https://doi.org/10.1016/S0166-4328\(99\)00044-3](https://doi.org/10.1016/S0166-4328(99)00044-3)
- Fell, J., & Axmacher, N. (2011). The role of phase synchronization in memory processes. *Nature Reviews Neuroscience*, 12(2), 105–118. <https://doi.org/10.1038/nrn2979>
- Foa, E. B. (2000). Psychosocial treatment of posttraumatic stress disorder. *The Journal of Clinical Psychiatry*, 61 Suppl 5, 43–48. <http://www.ncbi.nlm.nih.gov/pubmed/10761678>
- Fries, P. (2015). Communication through coherence. *Neuron*, 88(1), 220–235. <https://doi.org/10.1016/j.neuron.2015.09.034>
- Hanslmayr, S., Axmacher, N., & Inman, C. S. (2019). Modulating human memory via entrainment of brain oscillations. *Trends in Neurosciences*, 1–15. <https://doi.org/10.1016/j.tins.2019.04.004>
- Haselgrove, M., Aydin, A., & Pearce, J. M. (2004). A partial reinforcement extinction effect despite equal rates of reinforcement during pavlovian conditioning. *Journal of Experimental Psychology: Animal Behavior Processes*, 30(3), 240–250. <https://doi.org/10.1037/0097-7403.30.3.240>
- Headley, D. B., & Paré, D. (2017). Common oscillatory mechanisms across multiple memory systems. *Npj Science of Learning*, 2(1), 1. <https://doi.org/10.1038/s41539-016-0001-2>
- Herrmann, C. S., Strüber, D., Helfrich, R. F., & Engel, A. K. (2016). EEG oscillations: From correlation to causality. *International Journal of Psychophysiology*, 103, 12–21. <https://doi.org/10.1016/j.ijpsycho.2015.02.003>
- Herry, C., & Johansen, J. P. (2014). Encoding of fear learning and memory in distributed neuronal circuits. *Nature Neuroscience*, 17(12), 1644–1654. <https://doi.org/10.1038/nn.3869>
- Ho, J., Tumkaya, T., Aryal, S., Choi, H., & Claridge-Chang, A. (2019). Moving beyond P values: data analysis with estimation graphics. *Nature Methods*, 16(7), 565–566. <https://doi.org/10.1038/s41592-019-0470-3>
- Huerta, P. T., & Lisman, J. E. (1995). Bidirectional synaptic plasticity induced by a single burst during cholinergic theta oscillation in CA1 in vitro. *Neuron*, 15(5), 1053–1063. [https://doi.org/10.1016/0896-6273\(95\)90094-2](https://doi.org/10.1016/0896-6273(95)90094-2)
- Hyman, J. M., Wyble, B. P., Goyal, V., Rossi, C. A., & Hasselmo, M. E. (2003). Stimulation in



- hippocampal region CA1 in behaving rats yields long-term potentiation when delivered to the peak of theta and long-term depression when delivered to the trough. *Journal of Neuroscience*, 23(37), 11725–11731. <https://doi.org/10.1523/JNEUROSCI.23-37-11725.2003>
- Jiang, L., Wang, L., Yin, Y., Huo, M., Liu, C., Zhou, Q., Yu, D., Xu, L., & Mao, R. (2020). Spaced Training Enhances Contextual Fear Memory via Activating Hippocampal 5-HT2A Receptors. *Frontiers in Molecular Neuroscience*, 12(January), 1–8. <https://doi.org/10.3389/fnmol.2019.00317>
- Junghöfer, M., Elbert, T., Leiderer, P., Berg, P., & Rockstroh, B. (1997). Mapping EEG-Potentials on the surface of the brain: A strategy for uncovering cortical sources. *Brain Topography*, 9(3), 203–217. <https://doi.org/10.1007/bf01190389>
- Karalis, N., Dejean, C., Chaudun, F., Khoder, S., Rozeske, R., Wurtz, H., Bagur, S., Benchenane, K., Sirota, A., Courtin, J., & Herry, C. (2016). 4-Hz oscillations synchronize prefrontal-amygdala circuits during fear behavior. *Nature Neuroscience*, 19(4), 605–612. <https://doi.org/10.1038/nn.4251>
- Kim, W. Bin, & Cho, J. (2017). Encoding of discriminative fear memory by input-specific LTP in the amygdala. *Neuron*, 95(5), 1129–1146. <https://doi.org/10.1016/j.neuron.2017.08.004>
- King, A. J., & Palmer, A. R. (1985). Integration of visual and auditory information in bimodal neurones in the guinea-pig superior colliculus. *Experimental Brain Research*, 60(3), 492–500. <https://doi.org/10.1007/BF00236934>
- Kleiner, M., Brainard, D., Pelli, D., Ingling, A., Murray, R., & Broussard, C. (2007). What's new in Psychtoolbox-3 ? *Perception*, 36(ECVP Abstract Supplement).
- Knight, D. C., Nguyen, H. T., & Bandettini, P. A. (2003). Expression of conditional fear with and without awareness. *Proceedings of the National Academy of Sciences of the United States of America*, 100(25), 15280–15283. <https://doi.org/10.1073/pnas.2535780100>
- Knight, D. C., Nguyen, H. T., & Bandettini, P. A. (2006). The role of awareness in delay and trace fear conditioning in humans. *Cognitive, Affective and Behavioral Neuroscience*, 6(2), 157–162. <https://doi.org/10.3758/CABN.6.2.157>
- Lang, P. J., Davis, M., & Ohman, A. (2000). Fear and anxiety: animal models and human cognitive psychophysiology. *Journal of Affective Disorders*, 61(3), 137–159. [https://doi.org/10.1016/S0165-0327\(00\)00343-8](https://doi.org/10.1016/S0165-0327(00)00343-8)
- LeDoux, J. E. (2000). Emotion circuits in the brain. *Annual Review of Neuroscience*, 23(1), 155–184. <https://doi.org/10.1146/annurev.neuro.23.1.155>
- Lega, B. C., Jacobs, J., & Kahana, M. (2012). Human hippocampal theta oscillations and the formation of episodic memories. *Hippocampus*, 22(4), 748–761. <https://doi.org/10.1002/hipo.20937>
- Lennie, P. (1981). The physiological basis of variations in visual latency. *Vision Research*, 21(6), 815–824. [https://doi.org/10.1016/0042-6989\(81\)90180-2](https://doi.org/10.1016/0042-6989(81)90180-2)
- Lovibond, P. F., & Shanks, D. R. (2002). The role of awareness in Pavlovian conditioning: Empirical evidence and theoretical implications. *Journal of Experimental Psychology: Animal Behavior Processes*, 28(1), 3–26. <https://doi.org/10.1037/0097-7403.28.1.3>
- Luo, Q., Holroyd, T., Majestic, C., Cheng, X., Schechter, J., & James Blair, R. (2010). Emotional automaticity is a matter of timing. *Journal of Neuroscience*, 30(17), 5825–5829. <https://doi.org/10.1523/JNEUROSCI.BC-5668-09.2010>
- Lynch, M. A. (2004). Long-term potentiation and memory. *Physiological Reviews*, 84, 87–

136. <https://doi.org/https://doi.org/10.1152/physrev.00014.2003>
- 962 Maren, S., & Fanselow, M. (1995). Synaptic plasticity in the basolateral amygdala induced by  
 963 hippocampal formation stimulation in vivo. *The Journal of Neuroscience*, 15(11), 7548–  
 964 7564. <https://doi.org/10.1523/JNEUROSCI.15-11-07548.1995>
- 965 Markram, H., Lübke, J., Frotscher, M., & Sakmann, B. (1997). Regulation of synaptic efficacy  
 966 by coincidence of postsynaptic APs and EPSPs. *Science*, 275(5297), 213–215.  
 967 <https://doi.org/10.1126/science.275.5297.213>
- 968 McFadyen, J., Mermillod, M., Mattingley, J. B., Halász, V., & Garrido, M. I. (2017). A rapid  
 969 subcortical amygdala route for faces irrespective of spatial frequency and emotion.  
 970 *Journal of Neuroscience*, 37(14), 3864–3874.  
 971 <https://doi.org/10.1523/JNEUROSCI.3525-16.2017>
- 972 McTeague, L. M., Gruss, L. F., & Keil, A. (2015). Aversive learning shapes neuronal  
 973 orientation tuning in human visual cortex. *Nature Communications*, 6, 7823.  
 974 <https://doi.org/10.1038/ncomms8823>
- 975 Moratti, S., & Keil, A. (2005). Cortical activation during Pavlovian fear conditioning depends  
 976 on heart rate response patterns: An MEG study. *Cognitive Brain Research*, 25(2), 459–  
 977 471. <https://doi.org/10.1016/j.cogbrainres.2005.07.006>
- 978 Nokia, M. S., Waselius, T., Mikkonen, J. E., Wikgren, J., & Penttonen, M. (2015). Phase  
 979 matters: responding to and learning about peripheral stimuli depends on hippocampal  $\theta$   
 980 phase at stimulus onset. *Learning & Memory*, 22, 307–317.  
 981 <https://doi.org/10.1101/lm.038166.115>
- 982 Orsini, C. A., & Maren, S. (2012). Neural and cellular mechanisms of fear and extinction  
 983 memory formation. *Neuroscience & Biobehavioral Reviews*, 36(7), 1773–1802.  
 984 <https://doi.org/10.1016/j.neubiorev.2011.12.014>
- 985 Philips, G. T., Kopec, A. M., & Carew, T. J. (2013). Pattern and predictability in memory  
 986 formation: From molecular mechanisms to clinical relevance. *Neurobiology of Learning  
 987 and Memory*, 105, 117–124. <https://doi.org/10.1016/j.nlm.2013.05.003>
- 988 Place, R., Farovik, A., Brockmann, M., & Eichenbaum, H. (2016). Bidirectional prefrontal-  
 989 hippocampal interactions support context-guided memory. *Nature Neuroscience*, 19(8),  
 990 992–994. <https://doi.org/10.1038/nn.4327>
- 991 Polanía, R., Nitsche, M. A., Korman, C., Batsikadze, G., & Paulus, W. (2012). The  
 992 importance of timing in segregated theta phase-coupling for cognitive performance.  
 993 *Current Biology*, 22(14), 1314–1318. <https://doi.org/10.1016/j.cub.2012.05.021>
- 994 Quirk, G. J., Repa, J. C., & LeDoux, J. E. (1995). Fear conditioning enhances short-latency  
 995 auditory responses of lateral amygdala neurons: Parallel recordings in the freely  
 996 behaving rat. *Neuron*, 15(5), 1029–1039. [https://doi.org/10.1016/0896-6273\(95\)90092-6](https://doi.org/10.1016/0896-6273(95)90092-6)
- 997 Romanski, L. M., Clugnet, M. C., Bordi, F., & LeDoux, J. E. (1993). Somatosensory and  
 998 auditory convergence in the lateral nucleus of the amygdala. *Behavioral Neuroscience*,  
 999 107(3), 444–450. <https://doi.org/10.1037/0735-7044.107.3.444>
- 1000 Sacco, T., & Sacchetti, B. (2010). Role of secondary sensory cortices in emotional memory  
 1001 storage and retrieval in rats. *Science*, 329, 649–656.  
 1002 <https://doi.org/10.1126/science.1183165>
- 1003 Seidenbecher, T., Laxmi, T. R., Stork, O., & Pape, H. (2003). Amygdalar and hippocampal  
 1004 theta rhythm synchronization during fear memory retrieval. *Science*, 301(5634), 846–  
 1005 850. <https://doi.org/10.1126/science.1085818>
- 1006 Sevenster, D., Beckers, T., & Kindt, M. (2014). Fear conditioning of SCR but not the startle

- 1007 reflex requires conscious discrimination of threat and safety. *Frontiers in Behavioral*  
1008 *Neuroscience*, 8. <https://doi.org/10.3389/fnbeh.2014.00032>
- 1009 Silverstein, D. N., & Ingvar, M. (2015). A multi-pathway hypothesis for human visual fear  
1010 signaling. *Frontiers in Systems Neuroscience*, 9(AUGUST), 1–20.  
1011 <https://doi.org/10.3389/fnsys.2015.00101>
- 1012 Skrandies, W. (2007). The effect of stimulation frequency and retinal stimulus location on  
1013 visual evoked potential topography. *Brain Topography*, 20(1), 15–20.  
1014 <https://doi.org/10.1007/s10548-007-0026-1>
- 1015 Steil, R., & Ehlers, A. (2000). *Posttraumatische Diagnoseskala (PDS)*. Psychologisches  
1016 Institut, Universität Jena.
- 1017 Summerfield, C., & Mangels, J. A. (2005). Coherent theta-band EEG activity predicts item-  
1018 context binding during encoding. *NeuroImage*, 24(3), 692–703.  
1019 <https://doi.org/10.1016/j.neuroimage.2004.09.012>
- 1020 Taub, A. H., Perets, R., Kahana, E., & Paz, R. (2018). Oscillations synchronize amygdala-to-  
1021 prefrontal primate circuits during aversive learning. *Neuron*, 97(2), 291–298.e3.  
1022 <https://doi.org/10.1016/j.neuron.2017.11.042>
- 1023 Thut, G., Schyns, P. G., & Gross, J. (2011). Entrainment of perceptually relevant brain  
1024 oscillations by non-invasive rhythmic stimulation of the human brain. *Frontiers in*  
1025 *Psychology*, 2(170), 1–10. <https://doi.org/10.3389/fpsyg.2011.00170>
- 1026 Violante, I. R., Li, L. M., Carmichael, D. W., Lorenz, R., Leech, R., Hampshire, A., Rothwell,  
1027 J. C., & Sharp, D. J. (2017). Externally induced frontoparietal synchronization modulates  
1028 network dynamics and enhances working memory performance. *ELife*, 6, 1–22.  
1029 <https://doi.org/10.7554/eLife.22001>
- 1030 Wang, D., Clouter, A., Chen, Q., Shapiro, K. L., & Hanslmayr, S. (2018). Single-trial phase  
1031 entrainment of theta oscillations in sensory regions predicts human associative memory  
1032 performance. *The Journal of Neuroscience*, 38(28), 6299–6309.  
1033 <https://doi.org/10.1523/JNEUROSCI.0349-18.2018>
- 1034 Weiss, S., & Rappelsberger, P. (2000). Long-range EEG synchronization during word  
1035 encoding correlates with successful memory performance. *Cognitive Brain Research*,  
1036 9(3), 299–312. [https://doi.org/10.1016/S0926-6410\(00\)00011-2](https://doi.org/10.1016/S0926-6410(00)00011-2)
- 1037 Zheng, J., Stevenson, R. F., Mander, B. A., Mnatsakanyan, L., Hsu, F. P. K., Vadera, S.,  
1038 Knight, R. T., Yassa, M. A., & Lin, J. J. (2019). Multiplexing of theta and alpha rhythms  
1039 in the amygdala-hippocampal circuit supports pattern separation of emotional  
1040 information. *Neuron*, 102(4), 887–898.e5. <https://doi.org/10.1016/j.neuron.2019.03.025>

## 1041 **Figure, Table, and Extended Data Legends**

### 1042 *Figures*

#### 1043 **Figure 1.**

1044 Experimental design: Stimuli, procedure, and the operationalization of in-phase vs. out-of-phase  
1045 groups. **(A)** Gabor gratings used as conditioned stimuli (CS). The 45° grating served as CS+, (paired  
1046 with the unconditioned stimulus [US] during acquisition). The other 4 served as CS- (never paired with  
1047 the US). The luminance of each CS was sinusoidally modulated at 4 Hz. The US was a broadband  
1048 white noise, amplitude modulated at 4 Hz and presented at a maximum of 96.5 dB(A).



1049 **(B)** Fear conditioning procedure with the learning phases habituation, fear acquisition and extinction  
1050 (day1) and delayed recall (day 2). Each CS grating was presented 12 times in each learning phase.  
1051 The US was only presented during fear acquisition (12 times co-terminating with the CS+). At the end  
1052 of day 2 the unimodal audio task comprised 75 presentations of the 4 Hz-modulated white noise (4 s  
1053 each) at a non-aversive volume (max = 70.4 dB[A]). Vertical lines below the time line indicate the  
1054 rating time points. Extended data **Figure 1-1** shows the specific trial orders 1 and 2 that were used.  
1055 **(C)** Operationalization of the in-phase group vs. out-of-phase group. Fear conditioning for both groups  
1056 was identical with the only exception that the in-phase group received the 12 CS+ US pairings during  
1057 acquisition without a phase shift (0°) and the out-of-phase group received the CS+ US pairings with a  
1058 phase shift of 90°, 180°, and 270° (4 trials each). In **(C)**, the top row shows a simplified depiction of a  
1059 CS changing luminance at 4 Hz for 750 ms. The bottom part of **(C)** shows the first 750 ms of an  
1060 overlapping CS+ US presentation for the two groups. The light grey curve shows the luminance of the  
1061 CS+ (each vertical line shows one step following the monitor's 85 Hz refresh rate). The black (0°  
1062 phase shift), dark grey (90°), yellow (180°), and blue (270°) graphs show a down-sampled  
1063 representation of the 4 Hz modulated, white noise US.  
1064

#### 1065 **Figure 2.**

1066 Processing steps and validation of in-phase vs. out-of-phase stimulation. **(A)** Processing example (one  
1067 trial of one participant) of our audio (microphone in front of the participant's speakers) and video signal  
1068 (photo diode attached to the participants' monitor). Data were segmented relative to the onset of an  
1069 US (i.e., 12 segments per subject). Before analysis, video-data were shifted 40 ms forward in time to  
1070 account for the 40 ms time shift programmed into the stimulus presentation. Data were rectified, band-  
1071 pass filtered between 3 and 5 Hz and subjected to a Hilbert transform. Instantaneous phase  
1072 information at 4 Hz was extracted from the imaginary part of the analytic signal. **(B)** Visualization of in-  
1073 phase (left column) and out-of-phase (right column) CS+US stimulation for all CS+ US trials and all  
1074 participants (12 x 20 trials per group). Each thin orange line shows the video signal of one participant  
1075 and one trial. Each thin blue line shows the audio signal (one participant and trial). In **(B)**, the top rows  
1076 show band-pass filtered data, middle row shows the extracted phase information, at the bottom, polar  
1077 histograms show the clustering of all phase differences per group.

1078

#### 1079 **Figure 3.**

1080 ssVEP and ASSR 4 Hz signal in the time domain and frequency domain, as well as the scalp  
1081 distribution of the 4 Hz signal. The signal-to-noise ratio, averaged over all 40 participants (i.e.,  
1082 irrespective of factor group) is presented for the visual (A) and auditory (B) 4 Hz stimulation.

1083

#### 1084 **Figure 4.**

1085 Contrast weights. **(A)** Generalization weights to test the fit for a generalized fear response towards the  
1086 CS+ and neighboring CS- orientations, independent of the factor group. **(B)** Contrast weights  
1087 (discrimination) to test the group x orientation interaction. The weights shown for a narrow (blue) and  
1088 broad (orange) generalization pattern are just examples that if subtracted (narrow - broad) produce the  
1089 exact discrimination weights we used for the group x orientation interaction contrast (numbers in black  
1090 font, 0.142, -0.498, 0.694, -0.498, 0.142), resembling a 'Mexican hat' (black line).

1091

#### 1092 **Figure 5.**

1093 US-expectancy ratings separated for each measurement point: after acquisition, after extinction on  
1094 day 1, and before delayed recall on day 2 in the *in-phase* and the *out-of-phase* group. US-expectancy  
1095 was rated per CS on scale ranging from -5 (very certain, no US after this CS) over 0 (uncertain) to 5

1096 (very certain, an US will follow this CS). Each data point presents the mean US-expectancy rating for  
 1097 each CS orientation (averaged over participants per group and measurement point), error bars show  
 1098 one standard error of the mean (SEM).

1099 See Extended data **Figure 5-1** for discrimination indices (CS+ minus the weighted average of all CS-) and  
 1100 estimation statistics for US-expectancy ratings. For transparency Extended data **Figure 5-2**  
 1101 shows discrimination indices that result when subtracting the unweighted average of the CS- from the  
 1102 CS+.

1103

#### 1104 **Figure 6.**

1105 Valence ratings (**A**) and arousal ratings (**B**) separated for each measurement point: after habituation,  
 1106 after acquisition, after extinction (day 1), and before delayed recall (day 2). Valence was rated on a 9-  
 1107 point SAM scale from 1 (unpleasant) to 9 (pleasant). For better comparability with arousal ratings,  
 1108 valence ratings were recoded, changing the scale from 1 (pleasant) to 9 (unpleasant). Arousal was  
 1109 also rated on a 9-point SAM scale, here ranging from 1 (calm) to 9 (arousing). Each data point  
 1110 presents valence or arousal ratings, respectively, for each CS orientation (averaged over participants  
 1111 per group and measurement point), error bars show one standard error of the mean (SEM). Note: for  
 1112 better visualization y-axis is scaled from 3 to 8 instead of showing the full rating range from 1 to 9. See  
 1113 Extended data **Figure 6-1** for discrimination indices (CS+ minus the weighted average of all CS-) and  
 1114 estimation statistics of valence and arousal data. Extended data **Figure 6-2** additionally shows the  
 1115 discrimination indices that use the unweighted average of all CS- for subtraction.

1116

#### 1117 **Figure 7.**

1118 Single-trial (**A, B**) and averaged (**C**) skin conductance responses. Single-trial SCRs are separated by  
 1119 the synchronization condition into the in-phase, i.e., 0° phase offset (**A**) and out-of-phase group, i.e.,  
 1120 90°, 180°, 270° phase offset (**B**). Single-trial data are z-transformed SCRs, averaged over participants  
 1121 per group for each trial and CS-orientation. Before averaging, data was smoothed over the 12  
 1122 trials of a learning phase using a moving-average (5-points long, symmetrical, shrinking at the  
 1123 endpoints).

1124 (**C**) depicts averaged data over 12 trials of habituation, acquisition, extinction, and delayed recall to  
 1125 visualize the response patterns within each learning phase. Here, each data point presents z-  
 1126 transformed SCRs of each CS orientation averaged over participants and trials per group.

1127 Z-transformation was calculated with the means and standard deviations (SD) over CS and US  
 1128 responses of all learning phases (habituation, acquisition, immediate extinction, delayed recall) per  
 1129 participant. Error bars show  $\pm 1$  SEM. See Extended data **Figure 7-1** for single-trial SCR data without  
 1130 smoothing (i.e., no moving-average). **Figure 7-2** shows discrimination indices (CS+ minus weighted  
 1131 and average of all CS-) for SCR and estimation statistics. **Figure 7-3** depicts discrimination indices  
 1132 without weighting the averaged CS-.

1133

#### 1134 **Figure 8.**

1135 Single-trial (**A, B**) and averaged (**C**) power of the 4 Hz steady-state visually evoked potentials  
 1136 (ssVEPs) for each learning phase (habituation, acquisition, extinction, delayed recall). Single-trial data  
 1137 are separated by the synchronization condition into the in-phase, i.e., 0° phase offset (**A**) and the out-  
 1138 of-phase group, i.e., 90°, 180°, 270° phase offset (**B**).

1139 The ssVEP power is shown as SNR at 4 Hz, corrected for habituation level responding. Correction  
 1140 was done by dividing individual SNR values by the average SNR from habituation (mean over all 60  
 1141 trials of each participant, disregarding the different CS orientations). Therefore, values larger 1

1142 describe an enhancement and lower 1 a decrease of ssVEP-SNR at 4 Hz relative to habituation.  
 1143 Single trial data were smoothed over trials via a moving-average along the 12 trials of each learning  
 1144 phase (5-point symmetrical, shrinking at the endpoints). Each data point in **(A)** and **(B)** represents  
 1145 habituation corrected SNR for each trial and CS-orientation, averaged over participants per group.

1146 **(C)** depicts data averaged over the 12 trials of habituation, acquisition, extinction, and delayed recall  
 1147 to visualize the response patterns within each phase. Error bars show  $\pm 1$  SEM. Note: habituation data  
 1148 in **(C)** are nearly 'flat' around 1 due to the habituation correction, as described above and in the  
 1149 method section.

1150 Extended Data **Figure 8-1** shows single-trial data without the moving-average. **Figure 8-2** depicts  
 1151 discrimination indices with weighted CS- averages (CS+ minus weighted average of all CS-) and  
 1152 **Figure 8-3** was added for discrimination indices without weighting the averaged CS- responses.

1153

1154 **Tables**

1155 **Table 1.**

1156 **Summary of statistical analyses.** Table shows statistical analyses including *p* value and effect size  
 1157 for each memory outcome measure, separated by learning phase. For each outcome measure, we  
 1158 calculated repeated-measures ANOVAs with the CS orientation as within-subject factor and the group  
 1159 (in-phase vs. out-of-phase) as between-subject factor. Successful conditioning, i.e., increased  
 1160 response towards the CS+ respective of group) was validated by main effects of orientations (noted in  
 1161 the column effects as **ME: o**). To account for the specific symmetric generalization pattern (CS+ in the  
 1162 middle), additional generalization contrast fits were used (noted as **GEN**). Main effects of group (**ME:**  
 1163 **g**) and group x orientation interactions (**o x g INT**) addressed differences between in-phase and out-  
 1164 of-phase conditioning. Better grating discrimination vs. stronger generalization across orientations are  
 1165 described by a Mexican Hat contrast fit for the group x orientation interactions (MEX).

1166

1167

## 1168 *Extended Data*

### 1169 **Figure 1-1.**

1170 Table of trial list 1 and 2 for CS presentation order within each learning phase. The table shows the  
 1171 sequential order of conditioned stimulus (CS) presentation across the 60 trials of each learning phase.  
 1172 CS were Gabor-Gratings differing only in orientation (orientation degrees are shown in the 2<sup>nd</sup> to last  
 1173 columns). The 1<sup>st</sup> column (Trial) shows the sequential number (e.g., trial 2 was the 2<sup>nd</sup> CS seen by a  
 1174 participant in the specified learning phase). Each participant within the *in-phase* and *out-of-phase*  
 1175 *groups* was randomly assigned to receive stimuli according to list 1 or 2. Assignment to list 1 and 2  
 1176 was balanced across groups.

1177

1178

### 1179 **Figure 5-1.**

1180 Weighted discrimination indices for US-expectancy ratings. US-expectancy ratings were first z-  
 1181 transformed within each participant using the mean and SD of all US-expectancy ratings of a  
 1182 participant. With the z-transformed data we computed a *weighted discrimination index* per learning  
 1183 phase as the difference between the rating of the reinforced 45° (CS+) grating and the weighted  
 1184 average of the four CS- gratings. Weights for the CS- correspond to the angular difference in  
 1185 orientation between the four CS- (25°, 35°, 55°, 65°) and the CS+ (45°). The two more similar CS- (±  
 1186 10° to the CS+) were weighted with 0.33[...], while the more dissimilar orientations (± 20° to the CS+)  
 1187 were weighted with 0.166[...].

1188 Data and effect sizes are shown as a Cumming estimation plot (<http://www.estimationstats.com>) *Top*  
 1189 *row*: swarm plots show the raw discrimination indices per learning phase (each dot is the  
 1190 discrimination index of one participant). Group statistics are indicated to the right of each swarm as  
 1191 gapped lines (gap = mean, line length = 1 SD). *Bottom row*: effect size estimates (Hedges' *g*, black  
 1192 dots) for the 3 relevant comparisons (in-phase vs. out-of-phase for each learning phase) and their  
 1193 95% confidence interval (CI, vertical error bars).

1194 The unpaired Hedge's *g* for acquisition is -0.364 [95.0% CI -0.981 0.315] *p* = .2578; for extinction, -  
 1195 0.463 [CI -1.089 0.205] *p* = .1532, and for delayed recall, -0.249 [CI -0.907 0.370] *p* = .4206.

1196 5000 bootstrap samples were taken for CI estimation; the CI is bias-corrected and accelerated. The  
 1197 two-sided *P*-values are the likelihoods of observing the effect sizes, if the null hypothesis of zero  
 1198 difference is true. For each permutation *P*-value, 5000 reshuffles of the group labels were performed.

1199

1200

### 1201 **Figure 5-2.**

1202 Unweighted discrimination indices for US-expectancy ratings. US-expectancy ratings were z-  
 1203 transformed within each participant using the mean and SD of all US-expectancy ratings of a  
 1204 participant. The unweighted discrimination index shown is the difference between ratings of the CS+  
 1205 and the unweighted average of the four CS-. Data and effect sizes are shown as a Cumming  
 1206 estimation plot (<http://www.estimationstats.com>). See the legend of Extended data **Figure 5-1** for a  
 1207 detailed description of a Cumming estimation plot.

1208 The unpaired Hedge's *g* for acquisition is -0.306 [95% CI -0.928 0.375], *p* = .3356; for extinction, -  
 1209 0.372 [CI -1.021 0.289], *p* = .2346, and for delayed recall, -0.198 [CI -0.842 0.433], *p* = .5166. 5000  
 1210 bootstrap samples were taken for CI estimation; the CI is bias-corrected and accelerated. The two-  
 1211 sided *P*-values are the likelihoods of observing the effect sizes, if the null hypothesis of zero difference  
 1212 is true. For each permutation *P*-value, 5000 reshuffles of the group labels were performed.

1213

1214 **Figure 6-1.**

1215 Weighted discrimination indices for valence ratings **(A)** and arousal ratings **(B)**. Valence and arousal  
 1216 ratings were first z-transformed within each participant using the mean and SD of all ratings of valence  
 1217 and arousal of a participant, respectively. With the z-transformed data we computed a weighted  
 1218 discrimination index per learning phase as the difference between the reinforced 45° (CS+) grating  
 1219 and the weighted average of the four CS- gratings. Weights for the CS- correspond to the angular  
 1220 difference in orientation between the four CS- (25°, 35°, 55°, 65°) and the CS+ (45°): the two more  
 1221 similar CS- ( $\pm 10^\circ$  to the CS+) were weighted with 0.33[...], while the more dissimilar orientations ( $\pm$   
 1222 20° to the CS+) were weighted with 0.166

1223 Data and effect sizes are shown as a Cumming estimation plot (<http://www.estimationstats.com>). See  
 1224 the legend of Extended data **Figure 5-1** for a detailed description of a Cumming estimation plot.

1225 For valence data **(A)**, the unpaired Hedge's g for habituation is -0.039 [95.0% CI -0.680 0.568],  $p$   
 1226 = .896; for acquisition, -0.660 [CI -1.219 -0.048],  $p$  = .0372, for extinction, -0.291 [CI -0.925 0.354],  $p$  =  
 1227 .3522, and for delayed recall, -0.218 [CI -0.832 0.423],  $p$  = .4848. For arousal data **(B)**, the unpaired  
 1228 Hedge's g for habituation is -0.296 [CI -0.914 0.386],  $p$  = .3372; for acquisition, -0.877 [CI -1.459 -  
 1229 0.302],  $p$  = .0074, for extinction, -0.382 [CI -1.020 0.273],  $p$  = .2216, and for delayed recall, -0.142 [CI -  
 1230 0.778 0.510],  $p$  = .6472. 5000 bootstrap samples were taken for CI estimation; the CI is bias-corrected  
 1231 and accelerated. The two-sided  $P$ -values are the likelihoods of observing the effect sizes, if the null  
 1232 hypothesis of zero difference is true. For each permutation  $P$ -value, 5000 reshuffles of the group  
 1233 labels were performed.

1234

1235

1236 **Figure 6-2.**

1237 Unweighted discrimination indices for valence **(A)** and arousal **(B)** ratings. Ratings were z-transformed  
 1238 within each participant using the mean and SD of all valence and arousal ratings of a participant,  
 1239 respectively. The unweighted discrimination index shown is the difference between ratings of the CS+  
 1240 and the unweighted average of the four CS-. Data and effect sizes are shown as a Cumming  
 1241 estimation plot (<http://www.estimationstats.com>). See the legend of Extended data **Figure 5-1** for a  
 1242 detailed description of a Cumming estimation plot.

1243 For valence data **(A)**, the unpaired Hedge's g for habituation is 0.011 [95% CI -0.622 0.618]  $p$  = .9678;  
 1244 for acquisition, -0.578 [CI -1.153 0.047],  $p$  = .07, for extinction, -0.220 [CI -0.864 0.423],  $p$  = .488, and  
 1245 for delayed recall, -0.218 [CI -0.826 0.422],  $p$  = .485. For arousal data **(B)**, the unpaired Hedge's g for  
 1246 habituation is -0.255 [-0.866 0.439],  $p$  = .407; for acquisition, -0.820 [CI -1.424 -0.225],  $p$  = .0128, for  
 1247 extinction, -0.361 [CI -1.001 0.295],  $p$  = .2466, and for delayed recall, -0.141 [CI -0.774 0.503],  $p$  =  
 1248 .6512. 5000 bootstrap samples were taken for CI estimation; the CI is bias-corrected and accelerated.  
 1249 The two-sided  $P$ -values are the likelihoods of observing the effect sizes, if the null hypothesis of zero  
 1250 difference is true. For each permutation  $P$ -value, 5000 reshuffles of the group labels were performed.

1251

1252

1253 **Figure 7-1.**

1254 Single-trial data of skin conductance responses (SCRs) without smoothing over trials. Same data as in  
 1255 Figure 7 **(A, B)**, plotted without the moving-average over trials. SCRs are separated by learning phase  
 1256 (habituation, acquisition, extinction on day 1, and delayed recall on day 2) and by the synchronization  
 1257 condition into the in-phase, i.e., 0° phase offset **(A)** and out-of-phase group, i.e., 90°, 180°, 270°  
 1258 phase offset **(B)**. Error bars show  $\pm 1$  SEM.

1259

1260

1261 **Figure 7-2.**

1262 Weighted discrimination indices for averaged for averaged skin conductance responses (SCRs).  
 1263 SCRs were first z-transformed within each participant using the means and SD over CS and US



responses of all learning phases (habituation, acquisition, extinction, delayed recall). With the z-transformed data we computed a weighted discrimination index per learning phase as the difference between the reinforced 45° (CS+) grating and the weighted average of the four CS- gratings. Weights for the CS- correspond to the angular difference in orientation between the four CS- (25°, 35°, 55°, 65°) and the CS+ (45°): the two more similar CS- ( $\pm 10^\circ$  to the CS+) were weighted with 0.33[...], while the more dissimilar orientations ( $\pm 20^\circ$  to the CS+) were weighted with 0.166[...]. Data and effect sizes are shown as a Cumming estimation plot (<http://www.estimationstats.com>). See Extended data **Figure 5-1** legend for a detailed plot description. The unpaired Hedge's g for habituation is -0.249 [95.0% CI -0.827 0.371],  $p = .451$ ; for acquisition, -0.405 [CI -0.938 0.211],  $p = .2044$ , for extinction, 0.847 [CI 0.277 1.361],  $p = .0096$ , and for delayed recall, 0.535 [CI -0.091 1.056],  $p = .0916$ .

### Figure 7-3.

Unweighted discrimination indices for averaged skin conductance responses (SCRs). SCRs were z-transformed within each participant using the means and SD over CS and US responses of all learning phases (habituation, acquisition, extinction, delayed recall). The unweighted discrimination index shown is the difference between SCR to the CS+ and the unweighted average of the four CS-. Data and effect sizes are shown as a Cumming estimation plot (<http://www.estimationstats.com>). See Extended data **Figure 5-1** legend for a detailed plot description. The unpaired Hedge's g for habituation is -0.146 [95% CI -0.754 0.461],  $p = .6618$ ; for acquisition, -0.385 [CI -0.920 0.230],  $p = .2296$ , for extinction, 0.754 [CI 0.197 1.259],  $p = .0212$ , and for delayed recall, 0.549 [CI -0.071 1.059],  $p = .0848$ . 5000 bootstrap samples were taken for CI estimation; the CI is bias-corrected and accelerated. The two-sided  $P$ -values are the likelihoods of observing the effect sizes, if the null hypothesis of zero difference is true. For each permutation  $P$ -value, 5000 reshuffles of the group labels were performed.

### Figure 8-1.

Single-trial power of the 4 Hz steady-state visually evoked potentials (ssVEP) without smoothing over trials. Same data as **Figure 8 (A, B)**, plotted without the moving-average over trials. Single-trials are separated by learning phase (habituation, acquisition, extinction on day 1, and delayed recall on day 2) and by the synchronization condition into the in-phase, i.e., 0° phase offset (**A**) and out-of-phase group, i.e., 90°, 180°, 270° phase offset (**B**). Error bars show  $\pm 1$  SEM.

### Figure 8-2.

Weighted discrimination indices for steady-state visually evoked potentials (ssVEPs). Within each learning phase, using the habituation corrected SNR at 4 Hz (**Figure 8 C**) we computed a weighted discrimination index per learning phase as the difference between the reinforced 45° (CS+) grating and the weighted average of the four CS- gratings. Weights for the CS- correspond to the angular difference in orientation between the four CS- (25°, 35°, 55°, 65°) and the CS+ (45°): the two more similar CS- ( $\pm 10^\circ$  to the CS+) were weighted with 0.33[...], while the more dissimilar orientations ( $\pm 20^\circ$  to the CS+) were weighted with 0.166[...]. Data and effect sizes are shown as a Cumming estimation plot (<http://www.estimationstats.com>). See Extended data **Figure 5-1** legend for a detailed plot description. The unpaired Hedge's g for habituation is 0.008 [95.0% CI -0.652 0.633],  $p = .979$ ; for acquisition, -0.114 [CI -0.731 0.511],  $p = .7084$ , for extinction, 0.130 [CI -0.519 0.741],  $p = .683$ , and for delayed recall, 0.054 [CI -0.564 0.702],  $p = .08622$ . 5000 bootstrap samples were taken for CI estimation; the CI is bias-corrected and accelerated. The two-sided  $P$ -values are the likelihoods of observing the

1314 effect sizes, if the null hypothesis of zero difference is true. For each permutation  $P$ -value, 5000  
1315 reshuffles of the group labels were performed.

1316

1317

1318 **Figure 8-3.**

1319 Unweighted discrimination indices for ssVEPs. Here, the discrimination index was computed as the  
1320 difference between the reinforced 45° (CS+) grating and the unweighted average of the four CS-. Data  
1321 and effect sizes are shown as a Cumming estimation plot (<http://www.estimationstats.com>). See  
1322 Extended data **Figure 5-1** legend for a detailed plot description.

1323 The unpaired Hedge's  $g$  for habituation is -0.074 [95% CI -0.708 0.569],  $p = .8106$ ; for acquisition, -  
1324 0.161 [CI -0.774 0.464],  $p = .6074$ , for extinction, 0.080 [CI -0.561 0.706],  $p = .7948$ , and for delayed  
1325 recall, 0.044 [CI -0.579 0.687],  $p = .891$ . 5000 bootstrap samples were taken for CI estimation; the CI  
1326 is bias-corrected and accelerated. The two-sided  $P$ -values are the likelihoods of observing the effect  
1327 sizes, if the null hypothesis of zero difference is true. For each permutation  $P$ -value, 5000 reshuffles of  
1328 the group labels were performed.

1329

1330

**Table 1.**

**Summary of statistical analyses.** Table shows statistical analyses including  $p$  value and effect size for each memory outcome measure, separated by learning phase. For each outcome measure, we calculated repeated-measures ANOVAs with the CS orientation as within-subject factor and the group (in-phase vs. out-of-phase) as between-subject factor. Successful conditioning, i.e., increased response towards the CS+ respective of group) was validated by main effects of orientations (noted in the column effects as **ME: o**). To account for the specific symmetric generalization pattern (CS+ in the middle), additional generalization contrast fits were used (noted as **GEN**). Main effects of group (**ME: g**) and group x orientation interactions (**o x g INT**) addressed differences between in-phase and out-of-phase conditioning. Better grating discrimination vs. stronger generalization across orientations are described by a Mexican Hat contrast fit for the group x orientation interactions (MEX).

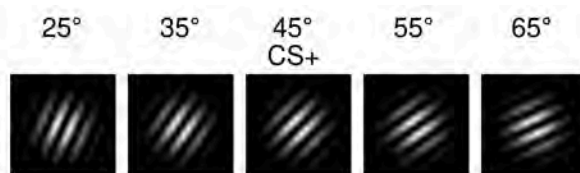
	Data structure	Type of test	Effects	Statistic	$p$ value	effect size
<b>US-expectancy</b>						
<i>Acquisition</i>						
a	normal	ANOVA	ME: o	$F_{(3,109)} = 12.491$	6.764E-7	$\eta^2_p = 0.247$
b	normal	ANOVA	GEN	$F_{(1,38)} = 28.360$	.000005	$\eta^2_p = 0.427$
c	normal	ANOVA	ME: g	$F_{(1,38)} = 7.310$	.010	$\eta^2_p = 0.161$
d	normal	ANOVA	o x g INT	$F_{(3,109)} = 1.133$	.338	$\eta^2_p = 0.029$
e	normal	ANOVA	MEX	$F_{(1,38)} = 4.796$	.035	$\eta^2_p = 0.112$
<i>Extinction</i>						
f	normal	ANOVA	ME: g	$F_{(1,38)} = 0.621$	.436	$\eta^2_p = 0.016$
g	normal	ANOVA	o x g INT	$F_{(3,113)} = 1.363$	.258	$\eta^2_p = 0.035$
h	normal	ANOVA	MEX	$F_{(1,38)} = 6.660$	.014	$\eta^2_p = 0.149$
<i>Delayed Recall (Day 2)</i>						
i	normal	ANOVA	ME: g	$F_{(1,36)} = 0.688$	.412	$\eta^2_p = 0.019$
j	normal	ANOVA	o x g INT	$F_{(3,100)} = 1.172$	.323	$\eta^2_p = 0.032$
k	normal	ANOVA	MEX	$F_{(1,36)} = 3.090$	.087	$\eta^2_p = 0.079$
<b>Valence &amp; Arousal</b>						
<i>Acquisition</i>						
l	normal	ANOVA <sub>Val</sub>	ME: o	$F_{(3,96)} = 7.756$	.000272	$\eta^2_p = 0.170$
m	normal	ANOVA <sub>Aro</sub>	ME: o	$F_{(3,100)} = 10.928$	.000008	$\eta^2_p = 0.223$
n	normal	ANOVA <sub>Val</sub>	GEN	$F_{(1,38)} = 12.354$	.001	$\eta^2_p = 0.245$
o	normal	ANOVA <sub>Aro</sub>	GEN	$F_{(1,38)} = 19.587$	.000078	$\eta^2_p = 0.340$
p	normal	ANOVA <sub>Val</sub>	ME: g	$F_{(1,38)} = 1.221$	.276	$\eta^2_p = 0.031$
q	normal	ANOVA <sub>Val</sub>	o x g INT	$F_{(3,96)} = 1.502$	.224	$\eta^2_p = 0.038$
r	normal	ANOVA <sub>Aro</sub>	ME: g	$F_{(1,38)} = 1.248$	.271	$\eta^2_p = 0.032$
s	normal	ANOVA <sub>Aro</sub>	o x g INT	$F_{(3,100)} = 1.658$	.187	$\eta^2_p = 0.042$
t	normal	ANOVA <sub>Val</sub>	MEX	$F_{(1,38)} = 9.228$	.004	$\eta^2_p = 0.195$
u	normal	ANOVA <sub>Aro</sub>	MEX	$F_{(1,38)} = 7.325$	.010	$\eta^2_p = 0.162$
<i>Extinction</i>						
v	normal	ANOVA <sub>Val</sub>	ME: g	$F_{(1,38)} = 1.810$	.186	$\eta^2_p = 0.045$
w	normal	ANOVA <sub>Val</sub>	o x g INT	$F_{(3,117)} = 0.647$	.590	$\eta^2_p = 0.017$



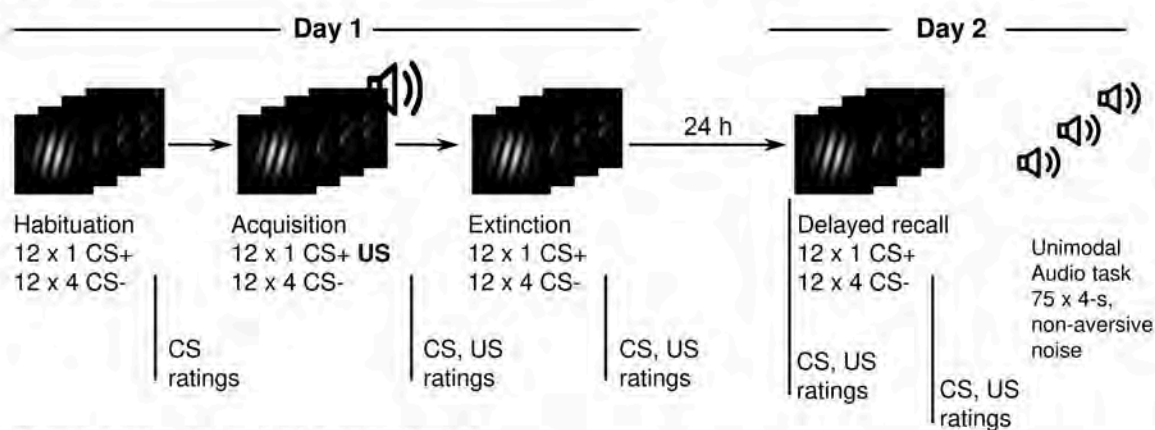
x	normal	ANOVA <sub>Aro</sub>	ME: g	$F_{(1,38)} = 0.355$	.555	$\eta^2_p = 0.009$
y	normal	ANOVA <sub>Aro</sub>	o x g INT	$F_{(3,112)} = 0.437$	.724	$\eta^2_p = 0.011$
<i>Delayed Recall (Day 2)</i>						
z	normal	ANOVA <sub>Val</sub>	ME: g	$F_{(1,36)} = 0.074$	.788	$\eta^2_p = 0.002$
aa	normal	ANOVA <sub>Val</sub>	o x g INT	$F_{(3,96)} = 0.216$	.864	$\eta^2_p = 0.006$
bb	normal	ANOVA <sub>Aro</sub>	ME: g	$F_{(1,36)} = 0.239$	.628	$\eta^2_p = 0.007$
cc	normal	ANOVA <sub>Aro</sub>	o x g INT	$F_{(3,100)} = .121$	.938	$\eta^2_p = 0.003$
<b>SCRs</b>						
<i>Acquisition</i>						
dd	normal	ANOVA	ME: o	$F_{(3,96)} = 14.856$	3.1057E-7	$\eta^2_p = 0.281$
ee	normal	ANOVA	GEN	$F_{(1,38)} = 31.987$	.000002	$\eta^2_p = 0.457$
ff	normal	ANOVA	ME: g	$F_{(1,38)} = 0.931$	.341	$\eta^2_p = 0.240$
gg	normal	ANOVA	o x g INT	$F_{(3,96)} = 0.833$	.461	$\eta^2_p = 0.021$
<i>Extinction</i>						
hh	normal	ANOVA	ME: g	$F_{(1,38)} = 1.170$	.286	$\eta^2_p = 0.030$
ii	normal	ANOVA	o x g INT	$F_{(3,117)} = 0.921$	.435	$\eta^2_p = 0.024$
<i>Delayed Recall (Day 2)</i>						
jj	normal	ANOVA	ME: g	$F_{(1,38)} = 0.002$	.965	$\eta^2_p = 0.00005$
kk	normal	ANOVA	o x g INT	$F_{(3,116)} = 1.483$	.222	$\eta^2_p = 0.038$
<b>ssVEPs</b>						
<i>Acquisition</i>						
ll	normal	ANOVA	ME: o	$F_{(4,137)} = 5.696$	.000479	$\eta^2_p = 0.130$
mm	normal	ANOVA	GEN	$F_{(1,38)} = 8.447$	.006	$\eta^2_p = 0.182$
nn	normal	ANOVA	o x g INT	$F_{(4,137)} = 1.042$	.384	$\eta^2_p = 0.027$
<i>Extinction</i>						
oo	normal	ANOVA	ME: g	$F_{(1,38)} = 2.957$	.094	$\eta^2_p = 0.072$
pp	normal	ANOVA	o x g INT	$F_{(4,147)} = 0.418$	.790	$\eta^2_p = 0.011$
<i>Delayed Recall (Day 2)</i>						
qq	normal	ANOVA	ME: g	$F_{(1,38)} = 5.354$	.026	$\eta^2_p = 0.123$
rr	normal	ANOVA	o x g INT	$F_{(3,122)} = 0.556$	.657	$\eta^2_p = 0.014$

Abbreviations: ANOVA = mixed repeated-measures ANOVA; ME = main effect; o=orientation;  $\eta^2_p$  = partial  $\eta^2$ ; g = group; MEX = Mexican Hat contrast fit of orientation x group interaction; INT = Interaction; GEN = Generalization fit; Val = Valence; Aro = Arousal

**A** Visual CS, five orientations



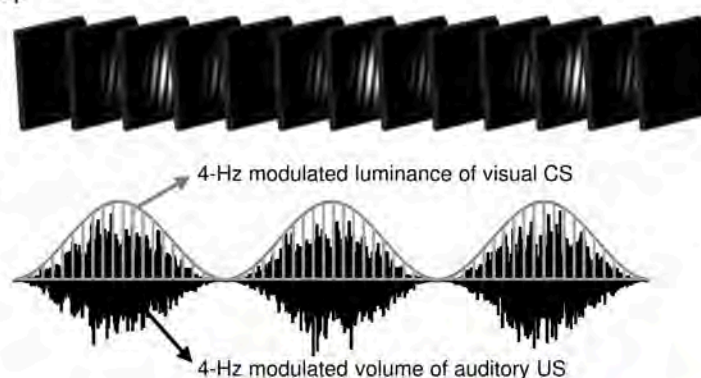
**B** Procedure



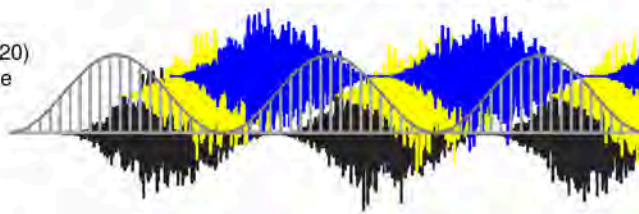
**C** In-phase group vs. out-of-phase group

Only for the 12 CS+US trials

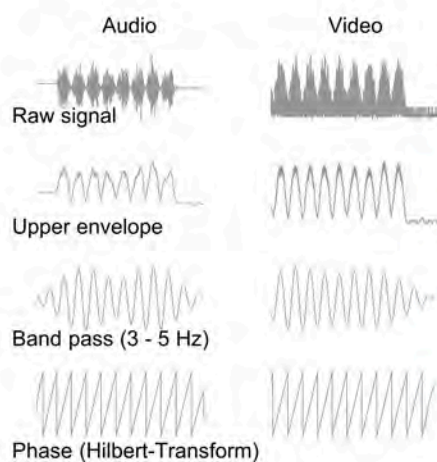
In-phase group ( $N = 20$ )



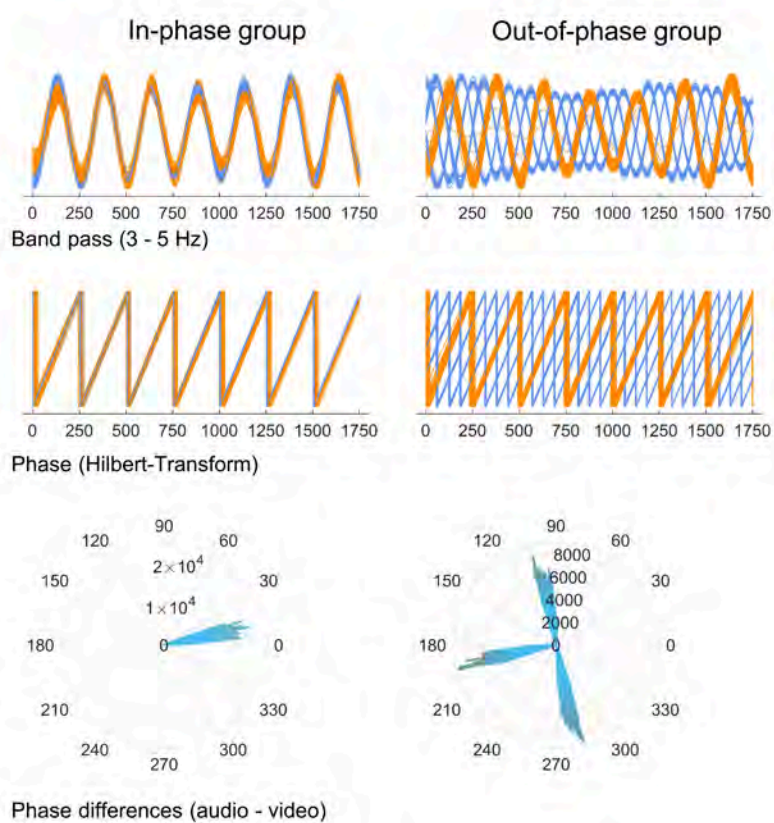
Out-of-phase group ( $N = 20$ )  
90°, 180°, and 270° phase offset



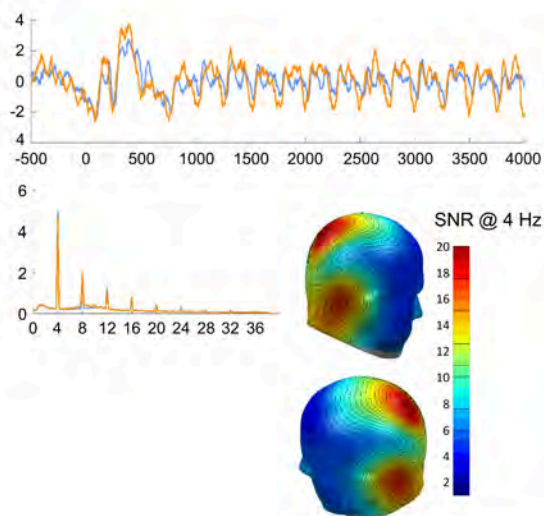
## A Processing example



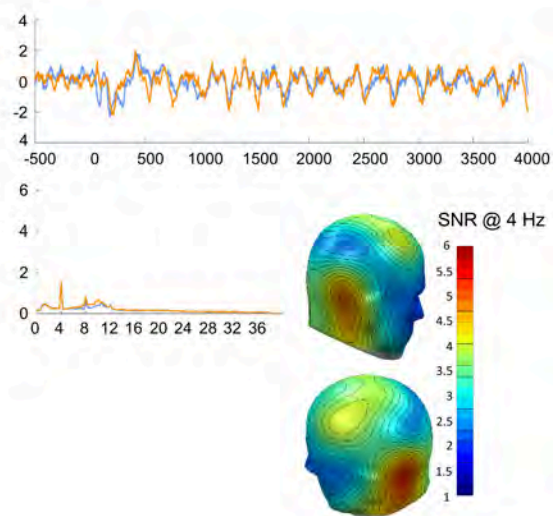
## B Stimulation validation



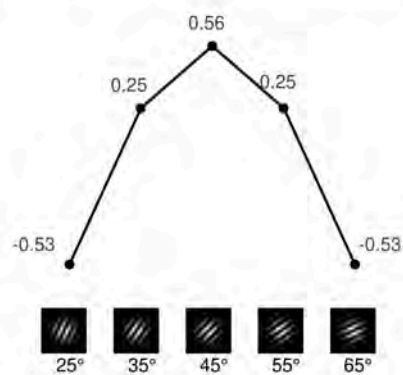
**A ssVEP**



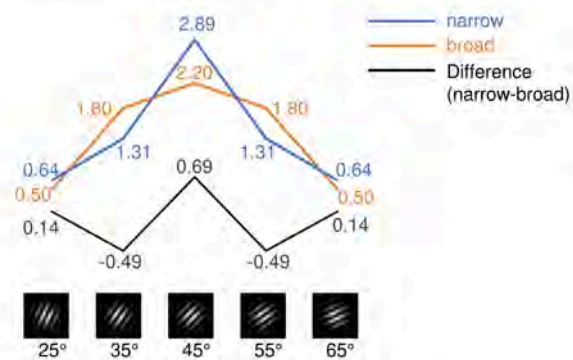
**B ASSR**

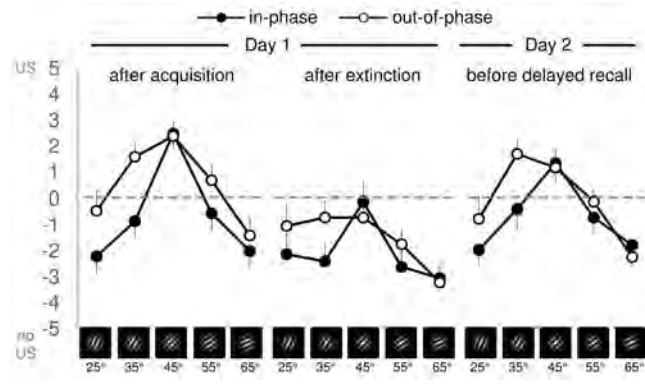


A) Model weights: generalization

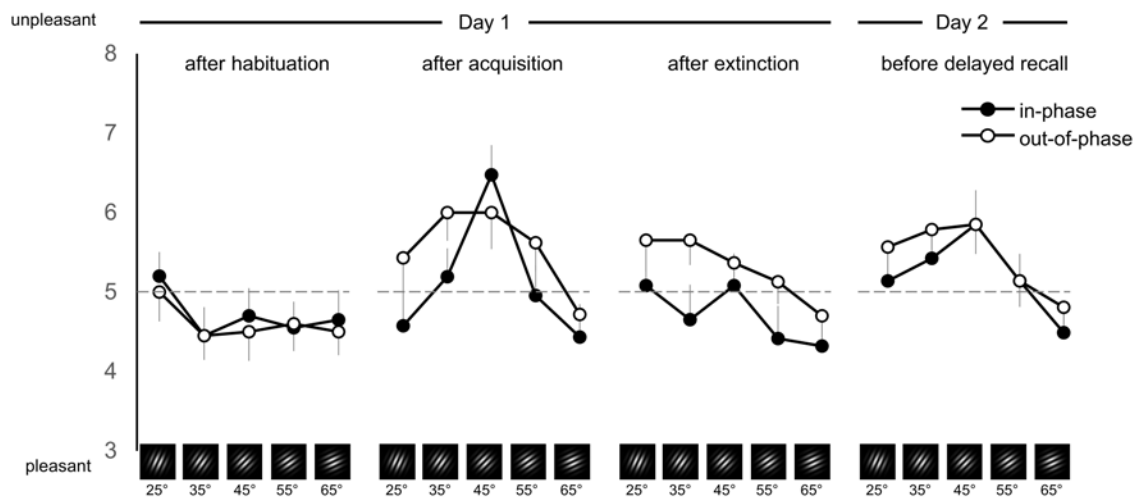


B) Interaction weights: Discrimination

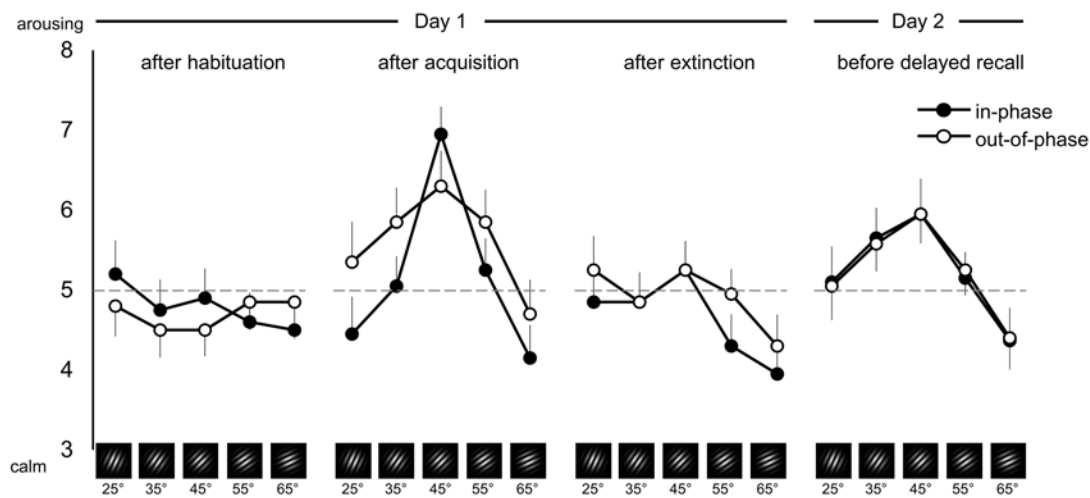




# (A) Valence ratings

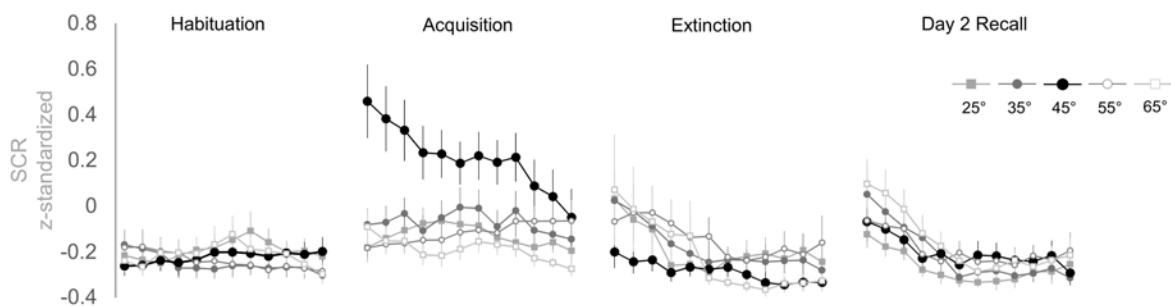


# (B) Arousal ratings

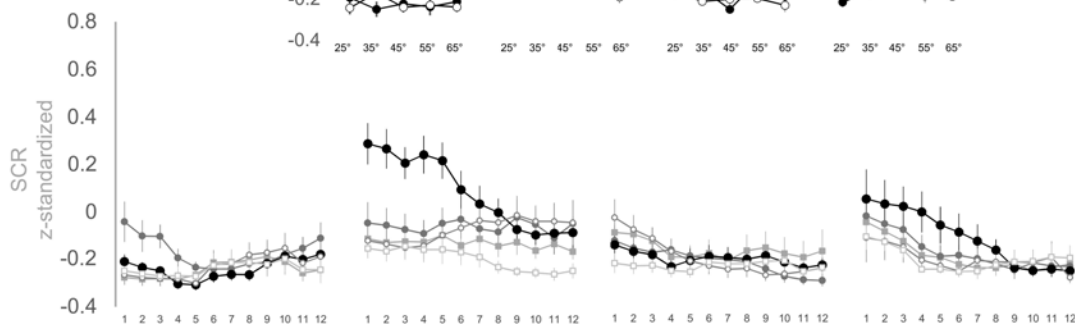




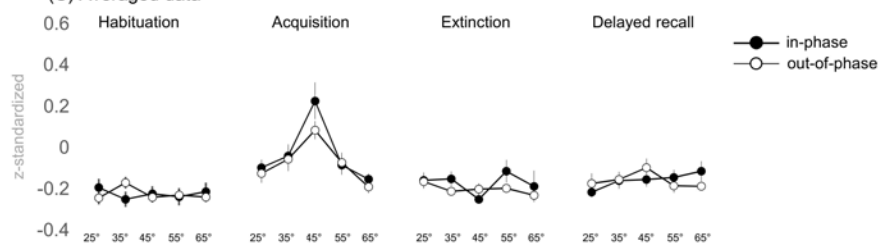
(A) In-phase group: 0° phase offset



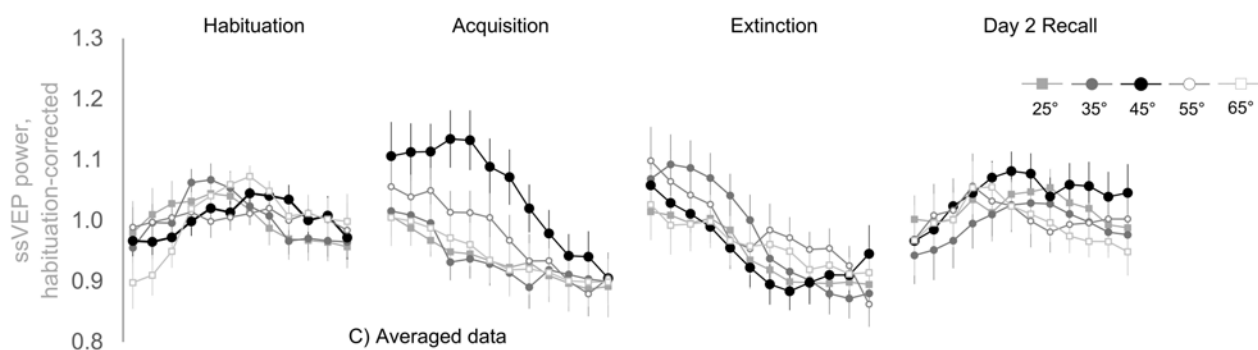
(B) Out-of-phase group: 90°, 180°, 270° phase offset



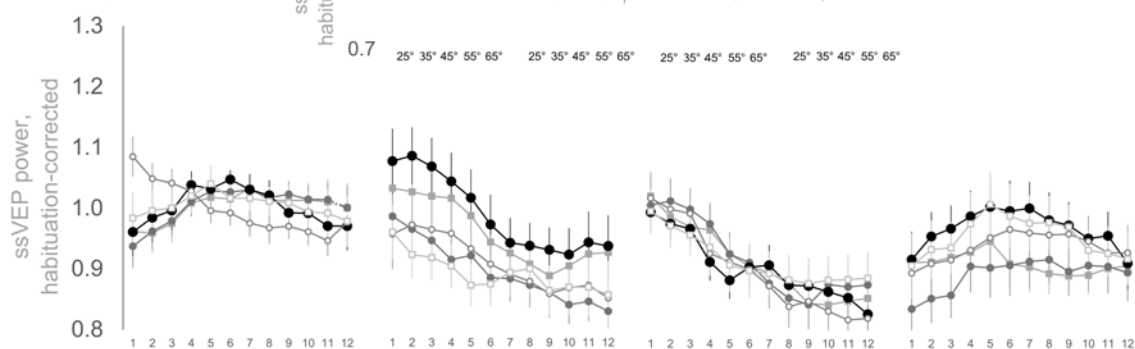
(C) Averaged data



(A) In-phase group: 0° phase offset



(B) Out-of-phase group: 90°, 180°, 270° phase offset



C) Averaged data

